Purpurinimide Carbohydrate Conjugates: Effect of the Position of the Carbohydrate Moiety in Photosensitizing Efficacy †

ARTICLE *in* MOLECULAR PHARMACEUTICS · JUNE 2007

Impact Factor: 4.38 · DOI: 10.1021/mp060135x · Source: PubMed

articles

molecular pharmaceutics

Purpurinimide Carbohydrate Conjugates: Effect of the Position of the Carbohydrate Moiety in Photosensitizing Efficacy†

Suresh K. Pandey,‡ Xiang Zheng,‡ Janet Morgan,§ Joseph R. Missert,‡ Ting-Hsiu Liu,|| Masayuki Shibata,|| David A. Bellnier,‡ Allan R. Oseroff,§ Barbara W. Henderson,‡ Thomas J. Dougherty,‡ and Ravindra K. Pandey*,‡

Photodynamic Therapy Center, Department of Dermatology, Roswell Park Cancer Institute, Buffalo, New York 14263, and Biomedical Informatics Program, Department of Health Informatics, UMDNJ-School of Health Related Professions, Newark, New Jersey 07107

Received December 28, 2006; Revised Manuscript Received January 31, 2007; Accepted February 15, 2007

Abstract: A lactose moiety was regioselectively introduced at various positions of *N*-hexyl-mesopurpurinimide (a class of chlorin containing a fused six-membered imide ring system, λ_{max}: 700 nm) to investigate the effect of its presence and position on photosensitizing efficacy. The resulting novel structures produced a significant difference in *in vitro* and *in vivo* efficacy. Among the positional isomers in which the lactose moiety was introduced at positions 3, 8, and 12, the 3-lactose purpurin-18-*N*-hexylimide produced the best efficacy. Compared to these analogues, the lactose moiety joined with an amide bond at position 17[2], and with an *N*-benzyl group bearing a −C≡C− linkage at position 13[2] showed reduced *in vitro/in vivo* photosensitivity. A noticeable difference between lactose conjugates in cell uptake (RIF tumor cells) was observed at 3 and 24 h postincubation. Replacing the lactose (Galβ1 → 4Glc) with β-galactose and glucose moieties at position 3 of purpurinimide produced an increase in both cell uptake and in *in vitro* efficacy, but with reduced *in vivo* efficacy. Sites of intracellular localization differed among photosensitizers with and without carbohydrate moieties. Molecular modeling shows favorable interactions of 3- and 12-lactose-purpurinimide analogues with both galectin-1 and galectin-3, but clear contributions were not found for the conjugate containing lactose moiety at position 8. In a comparative ELISA study of the lactose conjugates with free lactose, all carbohydrate-purpurinimides showed binding to both galectins with a significant variation between the batches of galectins.

Keywords: Photosensitizer (PS); carbohydrate; localization; phototoxicity; molecular modeling; photodynamic therapy (PDT)

Introduction

The major challenge in cancer therapy is the destruction of malignant cells while sparing the normal tissues. Among various choices for cancer treatment, photodynamic therapy (PDT) has a unique place and being noninvasive in nature makes it an increasingly desirable option. PDT involves the combination of visible light, photosensitizer, and tissue oxygen.[1] PDT is now widespread and is used clinically for treating various kinds maladies including cancer, age related macular degeneration, high-grade dysplasia (HGD) in Bar-

† Part of the work was presented at the ACS meeting (March 27−April 01) 2004, Anaheim, CA.

* Corresponding author. Mailing address: Chemistry Department/PDT Center, Roswell Park Cancer Institute, Elm and Carlton Streets, Buffalo, NY 14263. Phone: (716) 845-3203. Fax: (716) 845-8920. E-mail: ravindra.pandey@roswellpark.org.

‡ Photodynamic Therapy Center, Roswell Park Cancer Institute.

§ Department of Dermatology, Roswell Park Cancer Institute.

|| UMDNJ-School of Health Related Professions.

(1) (a) Henderson, B. W.; Dougherty, T. J. How does photodynamic therapy work? *Photochem. Photobiol.* **1992**, *55*, 145−157. (b) Dougherty, T. J.; Gomer, C. J.; Henderson, B. W.; Jori, G.; Kessel, D.; Korbelik, M.; Moan, J.; Pang, Q. Photodynamic therapy. *J. Natl. Cancer Inst.* **1998**, *90*, 889−905.

10.1021/mp060135x CCC: $37.00
Published on Web 03/21/2007

rett's esophagus, actinic keratoses, psoriasis, atherosclerosis (to remove plaque from arteries), jaundice in newborns, HIV, blood purification, mycosis fungoides, helicobacter pylori, etc.[2,3]

PDT achieves a certain degree of selectivity by moderate uptake and retention of photosensitizers and targeted light delivery to the tumor. However, the parameters currently chosen for optimized patient treatment are still limited by reactions of the normal tissue within the light field. Although the reasons for the accumulation of these compounds in tumors compared to normal tissue are not clearly understood, the balance between the hydrophilicity and lipophilicity has been recognized as an important feature.[4−6] One way to improve PDT efficacy is to design target specific photosensitizers by taking advantage of overexpression of specific receptors in tumor that discriminate tumor cells from normal healthy cells.[7] Conjugation of certain photosensitizers (e.g., chlorin e_6) with high molecular weight molecules such as adenovirus,[8] insulin-BSA,[9] microspheres,[10] BSA,[11] polylysine,[12] EGF-HSA,[13] immunoglobulin,[14] and many monoclonal antibodies has shown limited target specificity *in vivo* due to low delivery of the photosensitizers to the target site. Synthesis of homogeneous conjugates is a challenge, and typically nonuniform compositions are generated which complicates pharmacokinetic and pharmacodynamic characteristics.[15] Recent efforts with low molecular weight conjugates linking photosensitizers with cholesteryl oleate[16] or peptides[17] have shown some target specificity with LDL receptors and the cell nucleus respectively as targets.

In recent years, a variety of carbohydrate-conjugated photosensitizers have been synthesized and evaluated for PDT efficacy. Multivalent glycosylated conjugates of neutral, cationic,[18] dimeric[19] and strapped[20] amino acids incorporated analogues[21] of tetraphenyl porphyrins (TPP) have been tested in the K562 (human chronic myelogenous leukemia) cell line. Asymmetric neutral monomeric porphyrins having mono- or disaccharides showed more promise than symmetrical cationic and neutral porphyrin dimers bearing a higher number of saccharide units. Among these analogues, only amphiphilic TPP−carbohydrate conjugates had better efficacy than Photofrin.[22] In another comparative study on the

(2) (a) Dolmans, D. E.; Fukumura, D.; Jain, R. K. Photodynamic therapy for cancer. *Nat. Rev. Cancer* **2003**, *3*, 380−387. (b) Brown, S. B.; Brown, E. A.; Walker, I. The present and future role of photodynamic therapy in cancer treatment. *Lancet Oncol.* **2004**, *5*, 497−508.

(3) (a) Pandey, R. K.; Zheng, G. In *Porphyrin Handbook*; Smith, K. M., Kadish, K., Guilard, R., Eds.; Academic Press: San Diego, 2000; Vol. 6. (b) MacDonald, I. J.; Dougherty, T. J. Basic principles of photodynamic therapy. *J. Porphyrins Phthalocyanines* **2001**, *5*, 105−129.

(4) Henderson, B. W.; Bellnier, D. A.; Greco, W. R.; Sharma, A.; Pandey, R. K.; Vaughan, L. A.; Weishaupt, K. R.; Dougherty, T. J. An in vivo quantitative structure-activity relationship for a congeneric series of pyropheophorbide derivatives as photosensitizers for photodynamic therapy. *Cancer Res.* **1997**, *57*, 4000−4007.

(5) Moan, J.; Peng, Q.; Evenson, J. F.; Berg, K.; Western, A.; Rimington, C. Photosensitizing efficiencies, tumor- and cellular uptake of different photosensitizing drugs relevant for photodynamic therapy of cancer. *Photochem. Photobiol.* **1987**, *46*, 713−721.

(6) Banfi, S.; Caruso, E.; Buccafurni, L.; Murano, R.; Monti, E.; Gariboldi, M.; Papa, E.; Gramatica, P. Comparison between 5,-10,15,20-tetraaryl- and 5,15-diarylporphyrins as photosensitizers: synthesis, photodynamic activity, and quantitative structure-activity relationship modeling. *J. Med. Chem.* **2006**, *49*, 3293−3304.

(7) Sharman, W. M.; van Lier, J. E.; Allen, C. M. Targeted photodynamic therapy via receptor mediated delivery systems. *Adv. Drug Delivery Rev.* **2004**, *56*, 53−76.

(8) Akhlynina, T. V.; Jans, D. A.; Statsyuk, N. V.; Balashova, I. Y.; Toth, G.; Pavo, I.; Rosenkranz, A. A.; Naroditsky, B. S.; Sobolev, A. S. Adenoviruses synergize with nuclear localization signals to enhance nuclear delivery and photodynamic action of internalizable conjugates containing chlorin e6. *Int. J. Cancer* **1999**, *81*, 734−740.

(9) Akhlynina, T. V.; Rosenkranz, A. A.; Jans, D. A.; Sobolev, A. S. Insulin-mediated intracellular targeting enhances the photodynamic activity of chlorin e6. *Cancer Res.* **1995**, *55*, 1014−1019.

(10) Bachor, R.; Shea, C. R.; Gillies, R.; Hasan, T. Photosensitized destruction of human bladder carcinoma cells treated with chlorin e6-conjugated microspheres. *Proc. Natl. Acad. Sci. U.S.A.* **1991**, *88*, 1580−1584.

(11) Hamblin, M. R.; Miller, J. L.; Ortel, B. Scavenger-receptor targeted photodynamic therapy. *Photochem. Photobiol.* **2000**, *72*, 533−540.

(12) Soukos, N. S.; Hamblin, M. R.; Hasan, T. The effect of charge on cellular uptake and phototoxicity of polylysine chlorin(e6) conjugates. *Photochem. Photobiol.* **1997**, *65*, 723−729.

(13) Gijsens, A.; Missiaen, L.; Merlevede, W.; de Witte, P. Epidermal growth factor-mediated targeting of chlorin e6 selectively potentiates its photodynamic activity. *Cancer Res.* **2000**, *60*, 2197−2202.

(14) Gross, S.; Brandis, A.; Chen, L.; Belkin, V. R-.; Roehrs, S.; Scherz, A.; Salomon, Y. Protein-A-mediated targeting of bacteriochlorophyll-IgG to Staphylococcus aureus: a model for enhanced site-specific photocytotoxicity. *Photochem. Photobiol.* **1997**, *66*, 872−878.

(15) Savellano, M. D.; Hasan, T. Photochemical targeting of epidermal growth factor receptor: a mechanistic study. *Clin. Cancer Res.* **2005**, *11*, 1658−1668.

(16) Zheng, G.; Li, H.; Zhang, M.; Lund-Katz, S.; Chance, B.; Glickson, J. D. Low-density lipoprotein reconstituted by pyropheophorbide cholesteryl oleate as target-specific photosensitizer. *Bioconjugate Chem.* **2002**, *13*, 392−396.

(17) Bisland, S. K.; Singh, D.; Gariepy, J. Potentiation of chlorin e6 photodynamic activity in vitro with peptide-based intracellular vehicles. *Bioconjugate Chem.* **1999**, *10*, 982−992.

(18) Driaf, K.; Krausz, P.; Verneuil, B.; Spiro, M.; Blais, J. C.; Bolbach, G. Glycosylated cationic porphyrins as potential agents in cancer phototherapy. *Tetrahedron Lett.* **1993**, *34*, 1027−1030.

(19) Kaldapa, C.; Blais, J. C.; Carre, V.; Granet, R.; Sol, V.; Guilloton, M.; Spiro, M.; Krausz, P. Synthesis of new glycosylated neutral and cationic porphyrin dimers. *Tetrahedron Lett.* **2000**, *41*, 331−335.

(20) Davoust, E.; Granet, R.; Krausz, P.; Carre, V.; Guilloton, M. Synthesis of glycosyl strapped porphyrins. *Tetrahedron Lett.* **1999**, *40*, 2513−2516.

(21) Sol, V.; Blais, J.C.; Carre, V.; Granet, R.; Guilloton, M.; Spiro, M.; Krausz, P. Synthesis, Spectroscopy, and Photocytotoxicity of Glycosylated Amino Acid Porphyrin Derivatives as Promising Molecules for Cancer Phototherapy. *J. Org. Chem.* **1999**, *64*, 4431−4444.

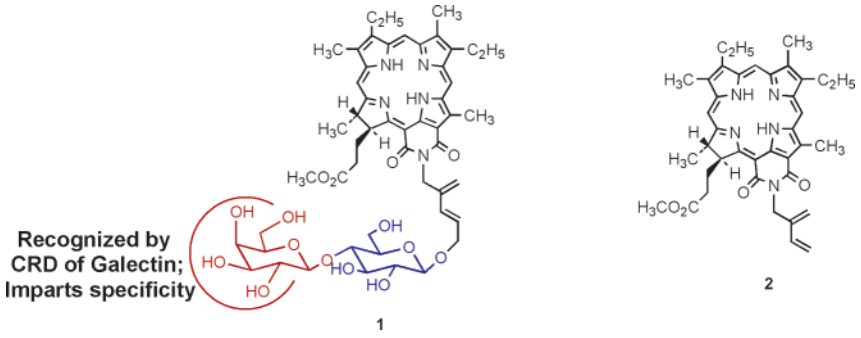

Figure 1. Structures of purpurinimide−lactose conjugate **1** and its precursor **2**.[30]

HT29 cell line it was found that asymmetric and amphiphilic TPC (*m*-O-GluOH)$_3$ enhanced phototoxicity 4-fold over the *m*-THPC (Foscan), while symmetric TPC (*m*-O-GluOH)$_4$ was poorly internalized and only weakly photoactive. TPC (*m*-O-GluOH)$_3$ was reported to be internalized by an active receptor-mediated endocytosis, and its higher phototoxicity has been correlated to its greater mitochondrial affinity.[23]

Since oligosaccharides play important roles in cellular communication through saccharide−receptor interactions,[24] which are usually specific and multivalent, their conjugation with a photosensitizer (PS) may confer high selectivity and specificity. Specificity of particular PS−saccharide conjugates for different cell lines have been shown by various groups. Fujimoto et al.[25] have reported that galactose conjugated TPP but not glucose conjugated TPP showed specificity for rat hepatoma RLC-16 cells (contains receptors for asialoglycoproteins). Chen et al.[26] have recently demonstrated specificity and selectivity of a tetraglucose conjugate of tetra (pentafluorophenyl)porphyrin linked by a sulfur atom over the corresponding tetra-galactose conjugate in human breast cancer cells (MDA-MB-231). On a 9L glioma rat model, Zhang et al.[27] have demonstrated that pyropheophorbide-2-deoxyglucosamide (Pyro-2DG) is transported and trapped in tumor cells (in mitochondria) via the glucose transporters/hexokinase pathway and can be utilized as a fluorescence imaging probe as well as a PDT agent.

Among the carbohydrate recognizing proteins, galectins (a subfamily of lectin) have unique features, which make them desirable targets for PDT via carbohydrate−photosensitizer conjugates.[28] The galectins have a highly conserved CRD domain with a high affinity for β-galactosides (for example lactose).[28] Compared to normal cells galectin-1 and galectin-3 expression in tumors may increase or decrease depending upon the cancer type,[29] which may play an important role for selective targeting.

In our previous study[30] a lactose(a β-galactoside)−chlorin conjugate with a diene linker was more effective *in vitro* compared to the precursor (Figure 1). In another previous study with a series of alkyl ether analogues of purpurinimides, we have shown that this system provides an "ideal"

(22) (a) Oulmi, D.; Maillard, P.; Guerquin-Kern, J. L.; Huel, C.; Momenteau, M. Glycoconjugated Porphyrins. 3. Synthesis of Flat Amphiphilic Mixed meso-(Glycosylated aryl)arylporphyrins and Mixed meso-(Glycosylated aryl)alkylporphyrins Bearing Some Mono- and Disaccharide Groups. *J. Org. Chem.* **1995**, *60*, 1554−1564. (b) Voszka, I.; Galantai, R.; Maillard, P.; Csik, G. Interaction of glycosylated tetraphenyl porphyrins with model lipid membranes of different compositions. *J. Photochem. Photobiol. B: Biol.* **1999**, *52*, 92−98.

(23) (a) Laville, I.; Figueiredo, T.; Loock, B.; Pigaglio, S.; Maillard, P.; Grierson, D. S.; Carrez, D.; Croisy, A.; Blais, J. Synthesis, cellular internalization and photodynamic activity of glucoconjugated derivatives of tri and tetra(meta-hydroxyphenyl)chlorins. *Bioorg. Med. Chem.* **2003**, *11*, 1643−1652. (b) Laville, I.; Pigaglio, S.; Blais, J. C.; Loock, B.; Maillard, P.; Grierson, D. S.; Blais, J. A study of the stability of tri(glucosyloxyphenyl)-chlorin, a sensitizer for photodynamic therapy, in human colon tumoural cells: a liquid chromatography and MALDI-TOF mass spectrometry analysis. *Bioorg. Med. Chem.* **2004**, *12*, 3673−3682. (c) Bautista-Sanchez, A.; Kasselouri, A.; Desroches, M. C.; Blais, J.; Maillard, P.; de Oliveira, D. M.; Tedesco, A. C.; Prognon, P.; Delaire, J. Photophysical properties of glucoconjugated chlorins and porphyrins and their associations with cyclodextrins. *J. Photochem. Photobiol. B* **2005**, *81*, 154−162.

(24) (a) Bertozzi, C. R.; Kiessling, L. L. Chemical glycobiology. *Science* **2001**, *291*, 2357−2363. (b) Rabinovich, G. A. Galectins: an evolutionarily conserved family of animal lectins with multifunctional properties; a trip from the gene to clinical therapy. *Cell Death Differ.* **1999**, *6*, 711−721. (c) Nangia-Makker, P.; Conklin, J.; Hogan, V.; Raz, A. Carbohydrate-binding proteins in cancer, and their ligands as therapeutic agents. *Trends Mol. Med.* **2002**, *8*, 187−192.

(25) Fujimoto, K.; Miyata, T.; Aoyama, Y. Saccharide-Directed Cell Recognition and Molecular Delivery Using Macrocyclic Saccharide Clusters: Masking of Hydrophobicity to Enhance the Saccharide Specificity. *J. Am. Chem. Soc.* **2000**, *122*, 3558−3559.

(26) Chen, X.; Hui, L.; Foster, D. A.; Drain, C. M. Efficient synthesis and photodynamic activity of porphyrin-saccharide conjugates: targeting and incapacitating cancer cells. *Biochemistry* **2004**, *43*, 10918−10929.

(27) Zhang, M.; Zhang, Z.; Blessington, D.; Li, H.; Busch, T. M.; Madrak, V.; Miles, J.; Chance, B.; Glickson, J. D.; Zheng, G. Pyropheophorbide 2-deoxyglucosamide: a new photosensitizer targeting glucose transporters. *Bioconjugate Chem.* **2003**, *14*, 709−714.

(28) Liu, F. T.; Rabinovich, G. A. Galectins as modulators of tumour progression. *Nat. Rev. Cancer* **2005**, *5*, 29−41.

(29) van den Brule, F.; Califice, S.; Castronovo, V. Expression of galectins in cancer: a critical review. *Glycoconjugate J.* **2004**, *19*, 537−542.

(30) Zheng, G.; Graham, A.; Shibata, M.; Missert, J. R.; Oseroff, A. R.; Dougherty, T. J.; Pandey, R. K. Synthesis of beta-galactose-conjugated chlorins derived by enyne metathesis as galectin-specific photosensitizers for photodynamic therapy. *J. Org. Chem.* **2001**, *66*, 8709−8716.

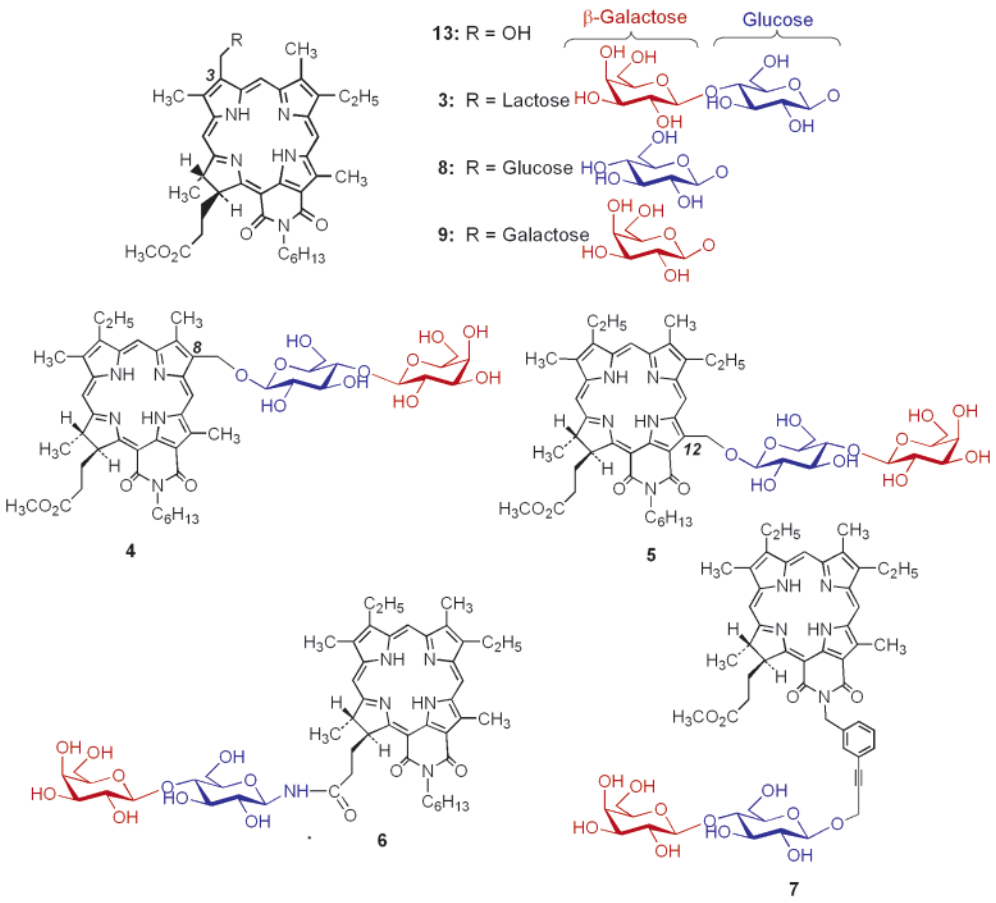

Figure 2. Synthetic purpurinimide−carbohydrate conjugates.

system to investigate structure−activity relationships by introducing substituents at various position(s) of the molecule.[31,32] This report describes the synthesis of a series of carbohydrate−PS conjugates with different chemical characteristics such as types of carbohydrate moieties, position of conjugation, type of linkers and their impact on intracellular localization and *in vitro/in vivo* efficacy.

Results and Discussion

Chemistry. For investigating the effect of the lactose moiety in photosensitizing activity, a series of purpurinimide−lactose conjugates in which the lactose moiety was joined with a diene linker **1** or regioselectively introduced at various positions of the purpurinimide system to produce the positional isomers **3**−**5** or linked with an amide (CONH) or ethylene (C≡C) bond **6** and **7** respectively were synthesized (Figure 2). Among these analogues, the conjugate containing the lactose moiety at position 3 showed the best efficacy (see the *in vitro* and *in vivo* results). Our next step was to investigate the impact of monosaccharides, and therefore, the corresponding glucose and galactose conjugates **8** and **9** respectively were also prepared. The structures of all the final conjugates and their acetylated precursors were confirmed by extensive 1H COSY, TOCSY and NOESY NMR studies, and the purity was ascertained by both reverse and normal phase HPLC analyses.

The key intermediate purpurin-18-methyl ester **10** (Scheme 1) was obtained from methylpheophorbide-a, which was isolated from *Spirulina pacifica*.[32] It was then converted into purpurin-18-*N*-hexylimide-17-propionic ester **11** by reacting with 1-hexylamine and a subsequent treatment with catalytic quantity of methanolic KOH and diazomethane.[32] The vinyl group present at position 3 of purpurinimide **11** was oxidized to the corresponding 3-formyl analogue **12** by reacting with osmium tetraoxide/sodium periodate,[33] which on reacting with sodium borohydride afforded 3-hydroxymethylpurpurin-

(31) Li, G.; Pandey, S. K.; Graham, A.; Dobhal, M. P.; Mehta, R.; Chen, Y.; Gryshuk, A.; Olson, K. R.; Oseroff, A.; Pandey, R. K. Functionalization of OEP-based benzochlorins to develop carbohydrate-conjugated photosensitizers. Attempt to target beta-galactoside-recognized proteins. *J. Org. Chem.* **2004**, *69*, 158−172.

(32) Zheng, G.; Potter, W. R.; Camacho, S. H.; Missert, J. R.; Wang, G.; Bellnier, D. A.; Henderson, B. W.; Rodgers, M. A. J.; Dougherty, T. J.; Pandey, R. K. Synthesis, photophysical properties, tumor uptake, and preliminary in vivo photosensitizing efficacy of a homologous series of 3-(1′-alkyloxy)ethyl-3-devinylpurpurin-18-N-alkylimides with variable lipophilicity. *J. Med. Chem.* **2001**, *44*, 1540−1559.

(33) Li, G.; Dobhal, M. P.; Shibata, M.; Pandey, R. K. Purpurinimide-fullerene dyads: introduction of fullerene moiety at various peripheral positions of the purpurinimide system. *Org. Lett.* **2004**, *6*, 2393−2396.

Scheme 1. Synthesis of Various Purpurinimides for the Preparation of Desired Purpurinimide−Carbohydrate Conjugates

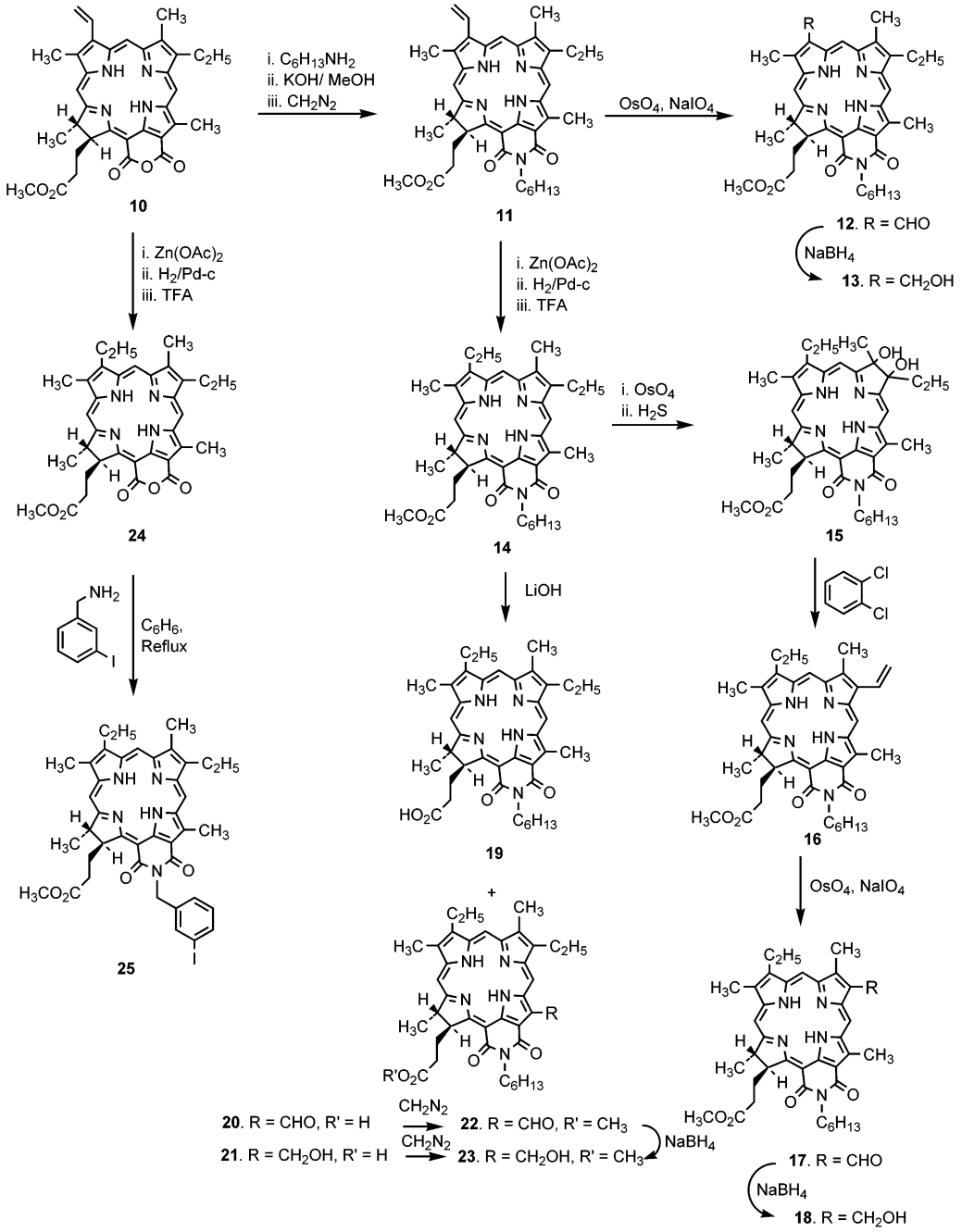

18-*N*-hexylimide-17-propionic ester **13** in a quantitative yield. In another set of experiments, using Pd/C as a catalyst the vinyl group at position 3 of purpurinimide **11** was hydrogenated to yield mesopurpurin-18-*N*-hexylimide-17-propionic ester **14** in a quantitative yield. The propionic ester functionality in compound **14** was hydrolyzed by aqueous lithium hydroxide to afford the corresponding 17-propionic acid derivative **19** as a major product along with a mixture 12-formyl mesopurpurin-18-*N*-hexylimide-17-propionic acid **20** and 12-hydroxymethyl mesopurpurin-18-*N*-hexylimide-17-propionic acid **21** as minor products, which on treating with diazomethane were converted into the respective methyl ester derivatives **22** and **23** (for the formation of the unexpected 12-formyl analogue **20** from **14** see ref 32). Sodium borohydride reduction of the formyl derivative **22** gave the corresponding hydroxymethyl analogue **23**.

Oxidation of purpurinimide **14** with osmium tetraoxide/hydrogen sulfide produced 7,8-dihydroxy-mesobacteriopurpurin-18-*N*-hexylimide-17-propionic ester **15**, which on acid-catalyzed dehydration afforded 8-vinyl derivative **16**.[33] The 8-vinylpurpurinimide **16** was oxidized to 8-formyl *meso*-

(34) Kozyrev, A. N.; Suresh, V.; Das, S.; Senge, M. O.; Shibata, M.; Dougherty, T. J.; Pandey, R. K. Syntheses and Spectroscopic Studies of Novel Chlorins with Fused Quinoxaline or Benzimidazole Ring Systems and the Related Dimers with Extended Conjugation. *Tetrahedron*, **2000**, *56*, 3353−3364.

Scheme 2. Synthetic Strategy for Linking the Carbohydrate Moiety at Different Position of the Purpurinimide System

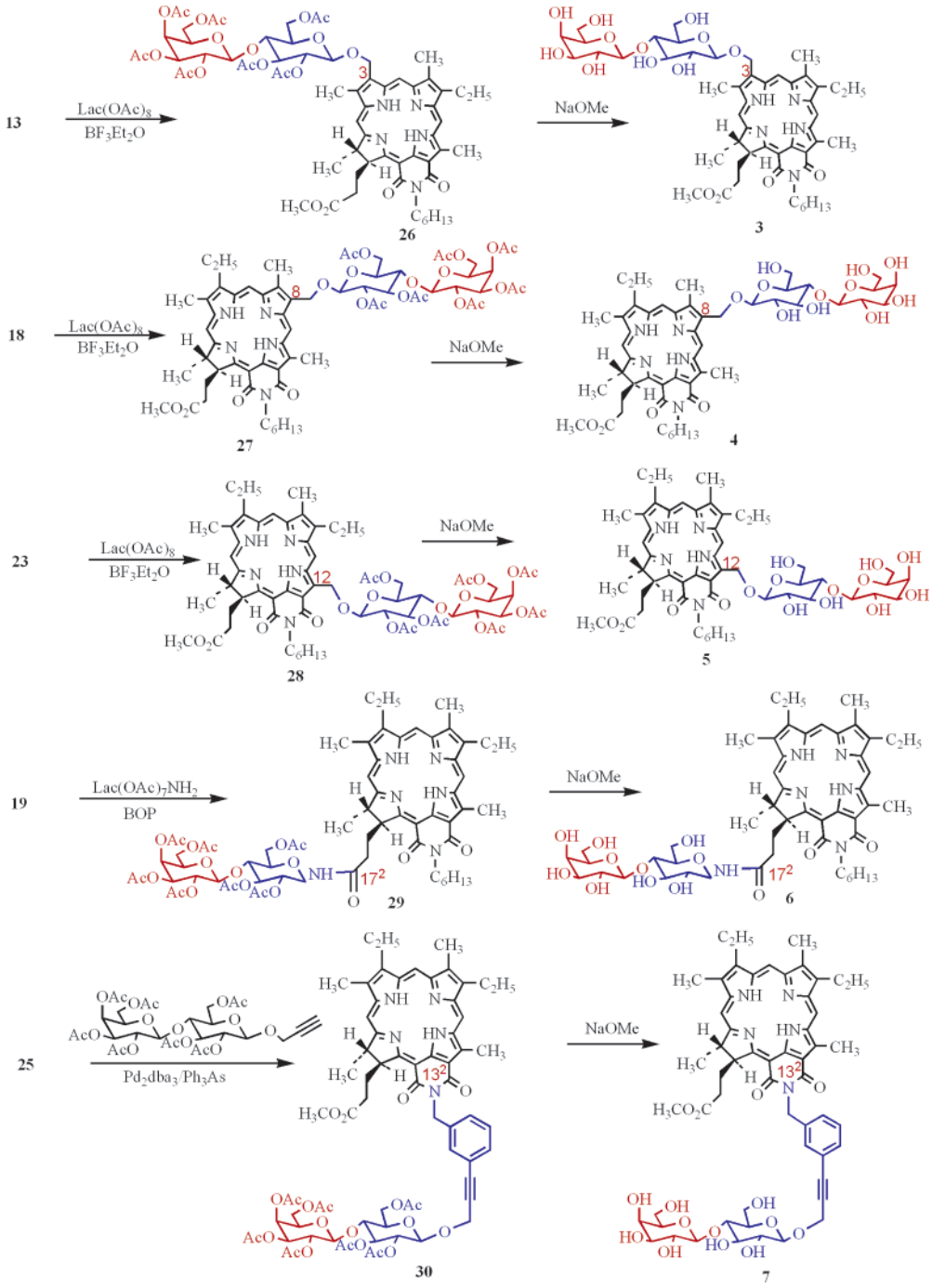

purpurin-18-*N*-hexylimide-17-propionic ester **17**, which upon reduction yielded 8-hydroxymethyl meso-purpurin-18-*N*-hexylimide-17-propionic ester **18** by following the methodology discussed above for the preparation of purpurinimide **23**. By following a similar approach, the purpurin-18-methyl ester **10** was converted in to *N*-(3-iodobenzyl) *meso*-purpurin-18-*N*-hexylimide-17-propionic ester **25** by hydrogenation over Pd/C followed by reacting the intermediate mesopurpurin-18-*N*-hexylimide-17-propionic ester **24** with 3-iodobenzylamine in refluxing benzene or toluene.

Compounds **13**, **18**, and **23** were reacted with lactose octaacetate in the presence of boron trifluoride diethyl etherate ($BF_3{\cdot}Et_2O$) to produce the corresponding intermediates **26**, **27**, and **28** respectively. Photosensitizer **19** was condensed with aminolactose heptaacetate in the presence of benzotriazol-1-yloxy-tris(dimethylamino)phosphonium hexafluorophosphate (BOP) to give intermediate **29**, while **25** was reacted with propargyllactose heptaacetate in the presence of tris(dibenzylidieneacetone)dipalladium(0) (Pd_2-dba_3) and triphenyl arsine (Ph_3As) to give compound **30**. Compounds **26**−**30** upon standard NaOMe/MeOH−CH_2Cl_2 deacetylation reaction conditions yielded the desired compounds **3**−**7** respectively in excellent quantity (Scheme 2).

Scheme 3. Preparation of Position 3 Substituted Galactose and Glucose *N*-Hexyl Purpurinimide Methyl Esters

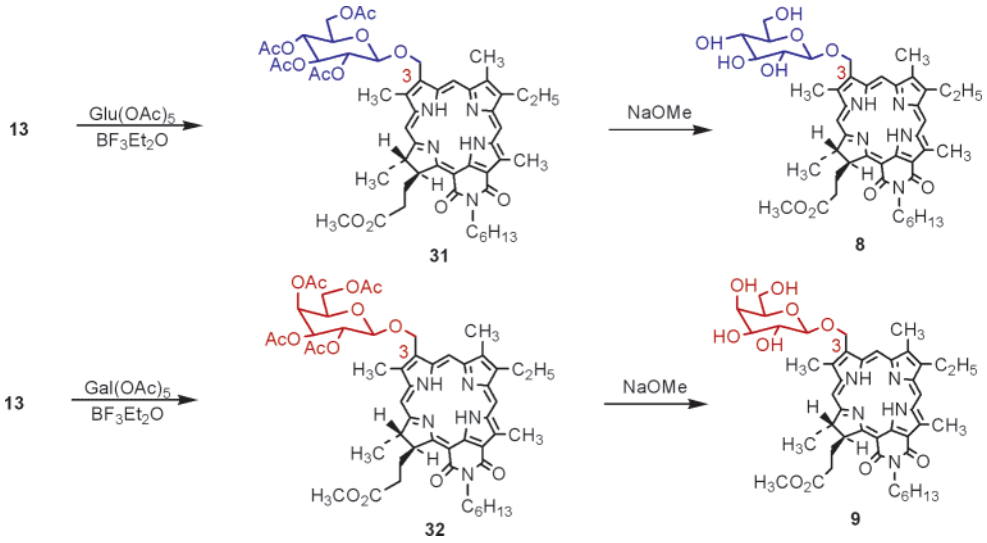

Table 1. log *P* Values of Certain Purpurinimides and the Corresponding Carbohydrate Conjugates at pH 7.0

	1	2	3	4	5	6	7	8	9	13
log *P*	1.88	6.16	2.40	2.40	2.99	2.70	3.12	4.45	4.45	6.05

Compound **13** was also reacted with glucose and galactose pentaacetate in the presence of boron trifluoride diethyl etherate ($BF_3{\cdot}Et_2O$) to produce the corresponding intermediates **31** and **32**, respectively, which upon deacetylation gave compounds glucose and galactose analogues **8** and **9** respectively in excellent yield (Scheme 3).

For determining a correlation between the overall lipophilicity in PDT efficacy, the log *P* values of all the final compounds were calculated using Pallas software (PALLAS, version 2.0, CompuDrug Chemistry Ltd.) and the results are summarized in Table 1.

***In Vitro* Photosensitizing Efficacy.** All compounds (purpurinimide and their carbohydrate conjugates) were insoluble in water and were formulated in 1% Tween 80/deionized water for biological evaluations except for compound **4**, which was formulated in 2% Tween 80/deionized water. However, compound **4** with lactose at position 8 showed severe dark cytotoxicity in RIF cells, above 0.5 μM due to the higher percentage of Tween 80 (Figure 3A).

Comparative *in vitro* studies were performed in RIF cells. Among the positional isomers **3**−**5**, compound **3** (LD_{50} = 0.21 μM, light dose; 1 J/cm^2) with lactose at position 3 was 4−5 times more potent than the isomers at position 8 (**4**: LD_{50} = 0.91 μM) and position 12 (**5**: LD_{50} = 0.84 μM) (Figure 3B and Table 2A). Compound **3** was also compared with lactose−purpurinimide conjugates linked by different linkers (**1**, **6**, and **7**) as well as with the nonconjugate purpurinimide **2** under similar experimental parameters, and as shown in Figure 3C, compound **3** showed the best efficacy. In a different set of experiments the photosensitizing

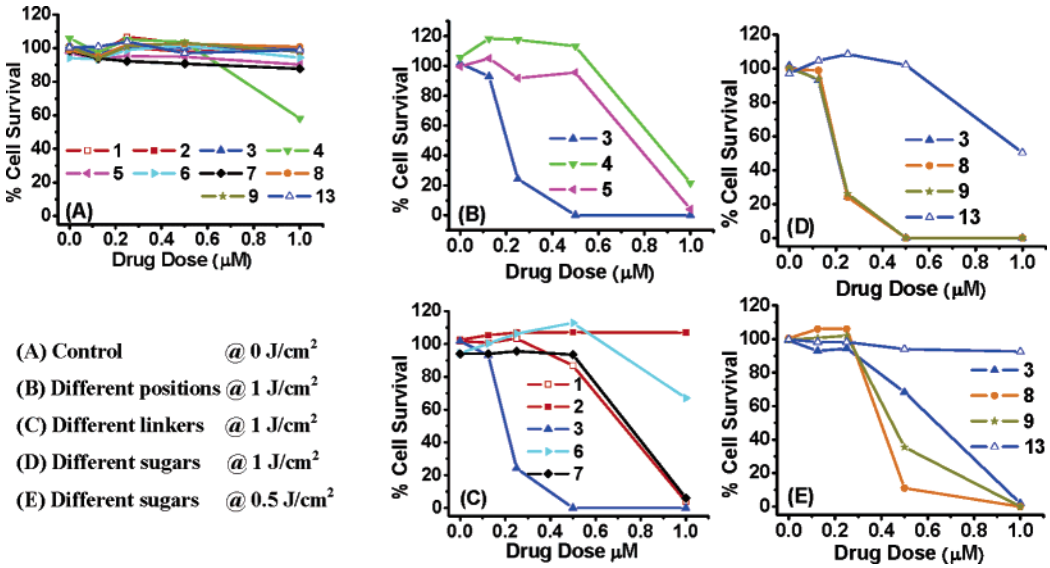

Figure 3. Comparative *in vitro* phototoxicity (MTT assay) activity for **1**−**9** and **13** at various drug doses in RIF tumor cells at 24 h postincubation.

Table 2. LD_{50} Values of Drug Dose (μM) in RIF Tumor Cell (Derived from Figure 3)

(A) Light Dose: 1 J/cm^2

	1	2	3	4	5	6	7	8	9	13
LD_{50}	>1.0	0.70	0.21	0.91[a]	0.84	> 1.0	0.85	0.21	0.21	1.0

(B) Light Dose: 0.5 J/cm^2

	3	8	9	13
LD_{50}	0.59	0.47	0.42	>1.0

[a] Dark cytotoxicity was found.

efficacy of the nonconjugate purpurinimide **13** and its corresponding lactose conjugate **3**, galactose **9** and glucose **8** conjugates was also investigated (Figure 3D). All carbohydrate−purpurinimide conjugates exhibited almost similar photosensitizing efficacy (LD_{50} = 0.21 μM) at 1 J/cm^2 light dose and were almost 5-fold more effective than their nonconjugate analogue **13** (LD_{50} = 1.0 μM). The results are summarized in Table 2A. To determine the difference in phototoxicity among the carbohydrate conjugates (**3**, **8**, and **9**), the light dose was reduced to 0.5 J/cm^2 (Figure 3E). Under such treatment parameters, the glucose conjugate **8** (LD_{50} = 0.42 μM) was more effective than the galactose **9** (LD_{50} = 0.47 μM) and lactose conjugate **3** (LD_{50} = 0.59 μM). Compared to the carbohydrate analogues, the nonconjugate purpurinimide **13** showed the least activity (LD_{50} >1.0 μM) (Table 2B).

Tumor Uptake. The *in vitro* uptake of the purpurinimide **13** and its corresponding carbohydrate conjugates were measured in RIF cells at 3 h and 24 h postincubation (Figure 4). At a short incubation period (3 h), lactose, glucose, and galactose conjugates **(3**, **8**, and **9** respectively**)** and the nonconjugated hydroxy methyl derivative **13** showed significantly higher tumor uptake than the rest of the purpurinimide−carbohydrate conjugates. At a longer incubation period (24 h), glucose **8** and galactose **9** conjugates showed a significant increase in tumor uptake compared to the lactose conjugate **3**. The overall uptake pattern was as follows: glucose-3 (**8**) > galactose-3 (**9**) > lactose-3 (**3**) > nonconjugate (**13**) > ethylene linked lactose-13^2 (**7**) > diene linked lactose-13^2 (**1**) > amide linked lactose-17^2 (**6**) > lactose-8 (**4**) > and lactose-12 (**5**).

***In Vivo* PDT Activity.** Carbohydrate−purpurinimide conjugates (**1**, **3**−**9**) and the nonconjugate (**13**) were evaluated for *in viv*o PDT activity in C3H mice bearing RIF tumors at two doses: 2.5 μmol/kg and 5.0 μmol/kg. The tumors were exposed to light (700 nm, 137 J/cm^2, 75 mW/cm^2) at 24 h postinjection. At 2.5 μmol/kg, no PDT response was observed (no data shown).

However, at 5.0 μmol/kg, among the positional isomers, compound **3** (lactose attached at position 3) produced the best long-term activity (Figure 5). Interestingly, under similar treatment conditions, the related glucose **8** and galactose **9** conjugates and nonconjugate **13** were ineffective. Among the lactose conjugates **1** and **3**, photosensitizer **3** showed better long-term activity (3/10 mice were tumor free on day 90).

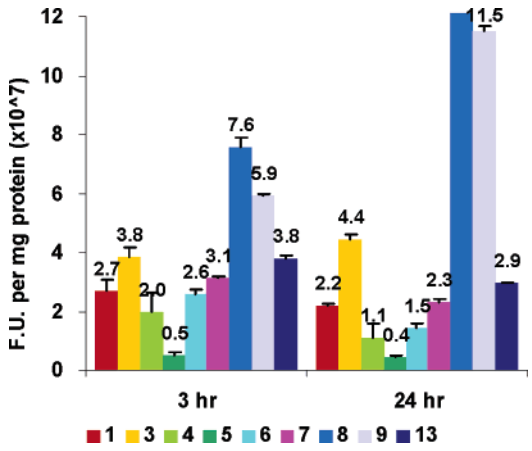

Figure 4. Comparative *in vitro* uptake of **1**, **3**−**9**, and **13** in RIF cells at short (3 h) and long (24 h) incubation period at 37 °C.

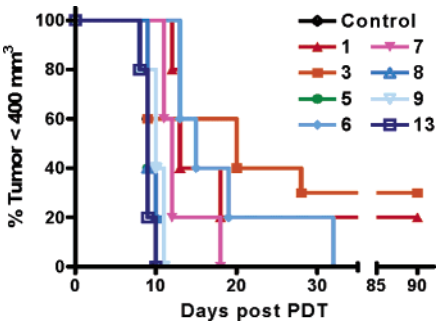

Figure 5. Comparative *in vivo* PDT efficacy (Kaplan−Meier plot) of purpurinimide−carbohydrate conjugates at a dose of 5.0 μmol/kg. The tumors were exposed with 700 nm.

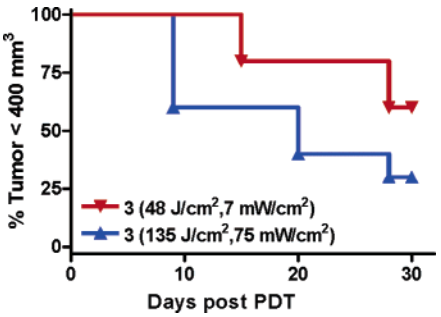

Figure 6. Comparative *in vivo* PDT efficacy (Kaplan−Meier plot) of **3** at dose of 5.0 μmol/kg. The mice were treated at different fluence rates at 24 h postinjection.

To investigate the effect of light dosimetry in photosensitizing efficacy, conjugate **3** was also evaluated under two light treatment conditions. In both treatment parameters, the drug dose was kept constant (5.0 μmol/kg) and the tumors were exposed at 24 h postinjection. As can be seen from Figure 6, under "low and slow" treatment conditions [light dose: 48 J/cm^2, 7 mW/cm^2 at 24 h postinjection), 60% mice were tumor free on day 30, which was significantly better than the results obtained from the "high and fast" treatment parameters (light dose: 135 J/cm^2, 75 mW/cm^2, 24 h postinjection, 3 out of 10 mice tumor free on day 30).

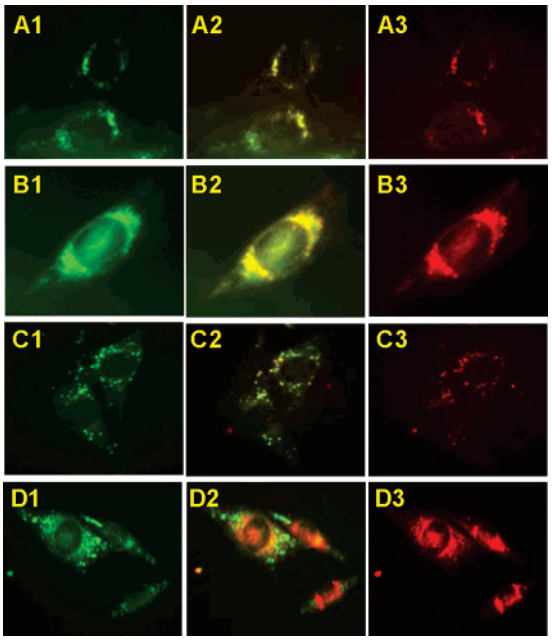

Figure 7. Comparative intracellular localization of **3** and **13** with Lyso Tracker (for Lysosome) and Bodipy C5 ceramide (for Golgi apparatus) in RIF cells 24 h postincubation. A1, B1: Bodipy C5 ceramide. A2, B2: overlay. A3: **3**. B3: **13**. C1, D1: Lyso Tracker. C2, D2: overlay. C3: **3**. D3: **13**.

Subcellular Localization. A difference in sites of localization was observed among photosensitizers with and without a carbohydrate moiety in RIF cells at 3 h and 24 h incubation. The details are summarized in Figure 7. In brief, the nonconjugate **13**, an ineffective photosensitizer, localized only in the Golgi apparatus, while the conjugated analogue **3**, an effective photosensitizer, was found in lysosomes as well as in the Golgi apparatus. None of these compounds showed mitochondrial localization.

Molecular Modeling. Interaction of Lactose−Purpurinimide Conjugates 3−5 (Positional Isomers) with Human Galectin-1 and Galectin-3 CRD. Among the β-galactoside recognizing proteins, galectin-1 (Gal-1) and galectin-3 (Gal-3) are widely studied due to their differential expression in tumor cells. In order to explore the molecular basis of the observed differences among various carbohydrate−purpurinimide conjugates in their *in vitro/in vivo* biological activities, a molecular modeling study was performed on the ligand−protein complexes.

Structure of Ligands. The semiempirical MO, AM1, energy optimized structures of compounds **3**, **4**, and **5** are shown in Figure 8. Since these structures are optimized *in vacuo*, the extended nature of these structures is clearly shown.

Structure of the Complexes. The crystal structures of human galectin-3 carbohydrate recognition domain (CRD) complexed with *N*-acetyl lactoseamine (PDB 1A3K)[35] and human galectin-1 complexed with lactose (PDB 1GZW)[36] were used as the templates to model galectin-3 ligand and galectin-1 ligand complexes, respectively. To model these complexes, the AM1 energy optimized purpurinimide−lactose conjugate must be placed on the carbohydrate-binding site of galectins. First, the six galactose ring atoms of lactose or lactoseamine for galectin-1 or galectin-3 complexes respectively were used as the references to bring the AM1 optimized purpurinimide−lactose conjugates. It became clear that the AM1 optimization process altered the lactose structure slightly from the one observed in crystals. The least-squares fitting procedure resulted in a well-superimposed galactose ring but, for some conjugates, the position of the glucose moiety with respect to galactose was somewhat different from one observed in the crystal. Since the contribution from the glucose moiety toward the lactose binding affinity for galectins is well established,[37] we decided to keep the crystal structures of the lactose moiety completely intact except for the link to the purpurinimides. This procedure eliminates the possible binding stability differences caused not by the interactions with the purpurinimide moiety but by the changes in interactions with the lactose moiety. Four glucose atoms (C1, O1, C2, and O5) at the conjugation site are used for superpositioning to create a composite purpurinimide−lactose conjugate at the binding site of galectins from the crystal structure of lactose and the AM1 energy optimized purpurinimide and linker. The superpositioning operations resulted in a good fit for all the compounds with the root-mean-square deviation values of around 0.05 Å. The resulting structures of the complexes clearly indicated that the purpurinimide moiety is far from the galactose-binding site due to its extended conformation resulting from AM1 optimization. However, it is expected that such a conformation would not be the most stable conformation at the interface of solvated proteins. Thus the systematic conformational search followed by energy minimization was performed for each compound against both galectin-1 and galectin-3. The systematic search results in several confor-

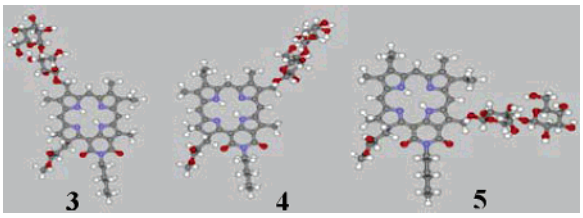

Figure 8.

(35) Seetharaman, J.; Kanigsberg, A.; Slabby, R.; Leffler, H.; Barondes, S. H.; Rini, J. M. X-ray crystal structure of the human galectin-3 carbohydrate recognition domain at 2.1-Å resolution. *J. Biol. Chem.* **1998**, *273*, 13047−13052.

(36) Lopez-Lucendo, M. F.; Solis, D.; Andre, S.; Hirabayashi, J.; Kasai, K.; Kaltner, H.; Gabius, H. J.; Romero, A. Growth-regulatory human galectin-1: crystallographic characterisation of the structural changes induced by single-site mutations and their impact on the thermodynamics of ligand binding. *J. Mol. Biol*. **2004**, *43*, 957−970.

(37) Hirabayashi, J.; Hashidate, T.; Arata, Y.; Nishi, N.; Nakamura, T.; Hirashima, M.; Urashima, T.; Oka, T.; Futai, M.; Muller, W. E.; Yagi, F.; Kasai, K. Oligosaccharide specificity of galectins: a search by frontal affinity chromatography. *Biochem. Biophys. Acta* **2002**, *1572*, 232−254.

Table 3. Relative Interaction Energy (in kcal/mol) between the Ligand and Galectin

	lactose[a]	conj **3**	conj **4**	conj **5**
galectin-1	0	−4.9	0.2	−4.4
galectin-3	0	−2.7	−1.1	−4.9

[a] The interaction energy of the lactose−galectin complex was taken as the reference, and the values shown above are the difference from the reference value. Thus, for example, compound **3** interacting with galectin-1 is 4.9 kcal/mol more stable than the interaction between lactose and galectin-1.

mations ranging from 9 to 31 in each Galectin. From these results, the major contributions to difference in stability come from the torsional angle differences in the linker regions since these angles dictate the relative orientation of the purpurinimide ring with respect to the carbohydrate recognition site. If the linker angles are identical, then the difference in the additional 10 dihedral angles within ethyl, 17-propionic ester, and *N*-hexylimide ring substituents does not contribute significantly to the stability. This is reasonable since all protein atoms are fixed in space without any flexibility of side chains. Thus one structure from each distinct conformational group of the linker was selected and was subjected to the MMFF94 based energy minimization. The change of force field was necessary since the Tripos force field used in the systematic conformational search often resulted in distorted chlorin rings for free chlorin systems. The crystal structures of lactose−galectin complexes were also subjected to partial energy optimization, which provides the reference value. The results of the interaction energy difference are summarized in Table 3.

From Table 3, it is clear that compounds **3** and **5** show favorable interactions with galectin-1 and galectin-3. Thus it shows that the linker position and purpurinimide contribute to additional binding stability of the purpurinimide−lactose conjugates to galectins. It is interesting to note that compound **5** shows strong interaction with both galectins. The lower in vitro and *in vivo* PDT activities for compound **5** compared to compound **3** may be attributed to its poor uptake (lowest among those examined, see Figure 4). On the other hand, these contributions were not clearly shown for compound **4**, which shows similar stabilities to the unconjugated lactose systems. However, it is not clear whether this is the intrinsic nature of this conjugate or alternatively an indication of restrictions imposed on the model construction. Clearly more sophisticated computational investigations are necessary to make a definite conclusion. The corresponding structures are shown in Figures 9 and 10 for galectin-1 and galectin-3 complexes, respectively. Although these calculations are still preliminary due to the restrictions imposed, nevertheless, it seems to indicate that the purpurinimide can contribute to the stability of the complex with galectins. This is consistent with the recent crystal structure analysis of galectin-3 CRD−2,3,5,6-tetrafluoro-4-methoxy-benzamine derivative of *N*-acetyllactose amine and various high-affinity galectin-3 inhibitors which suggest that the interaction between the aromatic ring of the lactose inhibitor and the positively charged residues of galectin-3 plays an important role in

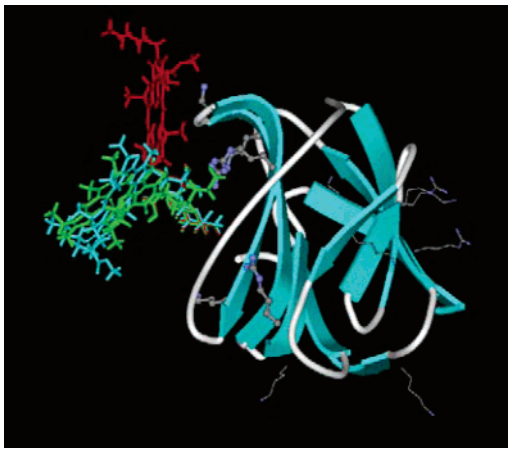

Figure 9. Interaction between human galectin-1 and purpurinimide−lactose conjugates. The conjugates are shown in stick with three different colors (red for compound **3**, cyan for compound **4**, and green for compound **5**). The galectin-1 is depicted schematically using secondary structures. The side chains of positively charged residues (arg and lys) are shown in line figures while those close to the conjugates are shown in ball and stick figures.

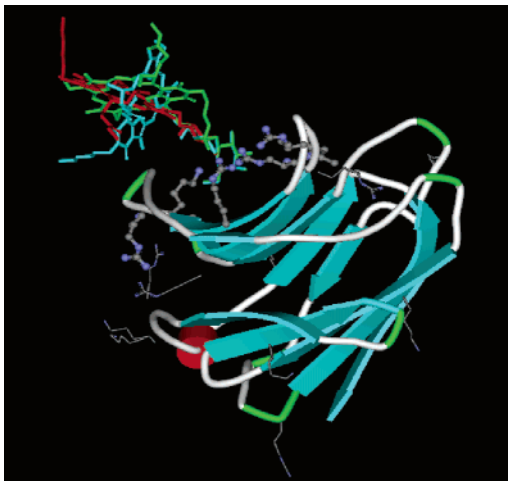

Figure 10. Structure of galectin-3 CRD interacting with carbohydrate−purpurinimide conjugates. The conjugates are shown in stick figures with three different colors (red for compound **3**, cyan for compound **4**, and green for compound **5**). The galectin-3 is depicted schematically using secondary structures. In the above figure, the side chains of all Arg and Lys residues are shown by line drawing. The Arg/Lys residues, which are close to the carbohydrate binding sites, are highlighted by stick and ball figures. We consider that these are residues, which might interact with the chlorin moiety resulting in enhanced binding to galectin-3.

enhanced binding.[38] It is interesting to note that a majority of the added stability on the complex with purpurinimide in

(38) Sorme, P.; Arnoux, P.; Kahl-Knutsson, B.; Leffler, H.; Rini, J. M.; Nilsson, U. J. Structural and thermodynamic studies on cation-Pi interactions in lectin-ligand complexes: high-affinity galectin-3 inhibitors through fine-tuning of an arginine-arene interaction. *J. Am. Chem. Soc.* **2005**, *127*, 1737−1743.

our calculations comes from the electrostatic contribution. More definitive complex structures and their ligand binding energetics will require additional calculations performed after removing various restrictions. The gal-1 and gal-3 binding affinities of the synthetic conjugates were also investigated by an ELISA method. In a comparative study with free lactose, all carbohydrate−purpurinimides produced significant binding to both galectins. Unfortunately, these results, although consistent within each batch, varied with different batches of galectins. Therefore, these findings are not presented.

Conclusions

We have developed a facile methodology for the synthesis of monocarbohydrate−purpurinimide conjugates that provides unique opportunity to prepare a series of *N*-alkyl/aryl analogues with variable lipophilicity. From the comparative *in vitro/in vivo* studies of a series of the positional isomers of lactose−purpurinimide conjugates, it was interesting to note a substantial difference in their photosensitizing efficacy. Among these analogues, the conjugate containing a lactose moiety at position 3 of the purpurinimide system was found to be most effective. Conjugating pyropheophorbide-a, purpurinimides, and bacteriopurpurinimides with those carbohydrate moieties known to have higher specificity for Gal-3 can further extend this approach, and these studies are currently in progress.

Molecular modeling studies of the galectin CRDs−purpurinimide−lactose conjugates showed a difference in binding affinity based on the position of lactose attachment on purpurinimide ring. Although various restrictions were imposed on the modeling of these complexes, it was evident that the purpurinimide moiety plays an important role toward enhanced binding to galectins, possibly due to its own interaction with the protein. Once the detailed *in vitro/in vivo* results are available with a series of compounds, it will be easier to correlate these findings with computational analysis. The galectin-1 and galectin-3 binding values for the carbohydrate conjugates obtained by ELISA showed higher binding affinity than the corresponding nonconjugate purpurinimides. However, these results varied with different batches of the galectins, and therefore, the specificity toward galectin-1 vs galectin-3 was not clearly established and requires additional studies.

Materials and Methods

Chemistry. All chemicals were of reagent grade and used as such. Solvents were dried using standard methods unless stated otherwise. Reactions were carried out under nitrogen atmosphere and were monitored by precoated (0.20 mm) silica TLC plastic sheet (20 × 20 cm) strips (POLYGRAM SIL N-HR) and/or UV−visible spectroscopy. Melting points were determined on a Fisher-Johns melting point apparatus and are uncorrected. UV−visible spectra were recorded on a Varian (Cary -50 Bio) spectrophotometer. ^{1}H NMR spectra were recorded on a Brucker AMX 400 and/or 600 MHz NMR spectrometer at 303 K in $CDCl_3$ or pyridine-d_5. All 2D ^{1}H NMR (ROESY, COSY, and TOCSY) were run on a Brucker AMX 600 MHz NMR spectrometer. Proton chemical shifts (δ) are reported in parts per million (ppm) relative to $CDCl_3$ (7.26 ppm) or pyridine-d_5 (8.74 ppm as the most downfield peak). Coupling constants (J) are reported in hertz (Hz), and s, d, t, q, p, m, and br refer to singlet, doublet, triplet, quartet, pentet, multiplet, and broad, respectively. Mass spectral data (Electro Spray Ionization, ESI by infusion) were obtained from Biopolymer Facility, Roswell Park Cancer Institute.

8^1-*O*-Lactose−Purpurin-18-*N*-hexylimide Conjugate (4). Yield: 90% (product was purified by passing through a short silica column using 25% MeOH in CH_2Cl_2 as eluant). Mp: 242−45 °C. UV−vis (THF): 690 (2.81×10^4), 639 (2.97×10^3), 543 (9.13×10^3), 507 (4.18×10^3), 417 (1.02×10^5), 363 (2.31×10^4). ^{1}H NMR (pyridine-d_5, 400 MHz): δ 10.46 (s, 1H, mesoH-10), 9.55 (s, 1H, mesoH-5), 8.82 (s, 1H, mesoH-20), 7.50 (brs, 1H, OH), 6.55 (brs, 2H, OH), 6.26 (d, J = 12.1, 1H, H-8^1), 6.00 (d, J = 12.4, 1H, H-8^1), 5.70 (brs, 2H, 2 × OH), 5.40 (d, J = 7.0, 1H, H-17), 5.17 (d, J = 7.9, 1H, lac.H), 4.94 (brs, 10H, 1 × lac.H, OH and H_2O), 4.75 (brs, 2H, lac.H), 4.67 (brs, 2H, lac.H), 4.41−4.60 (m, 6H, NCH_2(CH$_2$)$_4$CH$_3$ and lac.H), 4.34 (q, J = 8.7, 1H, H-18), 4.27 (t, J = 7.7, 1H, lac.H), 4.18−4.21 (m, 2H, lac. H), 4.09−4.12 (m, 1H, lac.H), 4.00 (s, 3H, CH$_3$-12), 3.75−3.79 (m, 2H, CH$_2$-3), 3.62 (s, 3H, CO$_2$CH$_3$-17^2), 3.28 (s, 3H, CH$_3$-2), 3.22 (s, 3H, CH$_3$-7), 3.00−3.05 (m, 1H, H-17^1), 2.75−2.85 (m, 2H, H-17^2 and H-17^1), 2.25−2.32 (m, 1H, H-17^2), 2.10−2.20 (m, 2H, NCH$_2$CH_2(CH$_2$)$_3$CH$_3$), 1.85 (t, J = 6.3, 3H, CH$_3$-18), 1.70 (t, J = 7.0, 3H, CH$_3$-3^1), 1.58−1.65 (m, 2H, N(CH$_2$)$_2$CH_2(CH$_2$)$_2$CH$_3$), 1.25−1.51 (m, 4H, N(CH$_2$)$_3$(CH_2)$_2$ CH$_3$), 0.89 (t, J = 6.0, 3H, N(CH$_2$)$_5$CH_3), 0.22 (brs, 1H, NH), 0.09 (brs, 1H, NH). Mass (ESI): 1012 (M^+ + Na).

12^1-*O*-Lactose−Purpurin-18-*N*-hexylimide Conjugate (5). Yield: 85% (the product was purified by passing through a short silica column using 25% MeOH in CH_2Cl_2 as eluant**)**. Mp: 225−27 °C. UV−vis (THF): 695 (3.77×10^4), 639 (7.97×10^3), 546 (1.79×10^4), 509 (5.78×10^3), 479 (3.87×10^3), 416 (1.01×10^5), 363 (4.12×10^4). ^{1}H NMR (20% CD_3OD in $CDCl_3$, 400 MHz): δ 9.84 (s, 1H, mesoH-10), 9.10 (d, J = 13.7, 1H, mesoH-5), 8.46 (s, 1H, mesoH-20), 6.51 (d, J = 12.2, 1H, H-12^1), 6.33 (d, J = 11.9, 1H, H-12^1), 5.27 (d, J = 8.8, 1H, H-17), 4.94 (d, J = 7.5, 1H, lac.H), 4.50 (brs, 7 × lac.OH and H_2O), 4.40−4.44 (m, 3H, NCH_2(CH$_2$)$_4$CH$_3$ and lac.H), 4.32 (q, J = 7.6, 1H, H-18), 4.06−4.09 (m, 1H, lac.H), 4.02 (dd,J=3.7, 9.6, 2H, lac.H), 3.81−3.88 (m, 2H, lac.H), 3.67−3.76 (m, 6H, lac.H), 3.58−3.65 (m, 4H, CH$_2$-3 and CH$_2$-8), 3.58 (s, 3H, CH$_3$-2), 3.50−3.54 (m, 1H, lac.H), 3.22 (s, 3H, CO$_2$CH$_3$-17^2), 3.14 (s, 3H, CH$_3$-7), 2.68−2.74 (m, 1H, H-17^1), 2.37−2.44 (m, 2H, H-17^2 and H-17^1), 1.92−2.02 (m, 3H, H-17^2 and NCH$_2$CH_2(CH$_2$)$_3$-CH$_3$), 1.75 (t, J = 7.3, 3H, CH$_3$-18), 1.71 (t, J = 7.6, 3H, CH$_3$-3^1), 1.65 (t, J = 7.8, 3H, CH$_3$-8^1), 1.57−1.62 (m, 2H, N(CH$_2$)$_2$CH_2(CH$_2$)$_2$CH$_3$), 1.41−1.47 (m, 4H, N(CH$_2$)$_3$(CH_2)$_2$

CH_3), 0.95 (t, $J = 7.1$, 3H, $N(CH_2)_5CH_3$). **Mass** (ESI): 1026 ($M^+ + Na$), 1004 (M^+).

17^2-Aminoacyllactose−Mesopurpurin-18-*N*-hexylimide Conjugate (6). Yield: 88% (the product was purified by passing through a short silica column using 25% MeOH in CH_2Cl_2 as eluant). Mp: 262−65 °C. UV−vis (THF): 693 (4.76×10^4), 638 (8.54×10^3), 543 (1.95×10^4), 507 (8.61×10^3), 416 (1.45×10^5), 362 (4.78×10^4). ^{1}H NMR (Py-d5, 400 MHz): δ 9.98 (s, 1H, mesoH-10), 9.79 (s, 1H, mesoH-5), 9.57 (s, 1H, mesoH-20), 8.71 (s, 1H, CONH), 5.95 (t, $J = 9.1$, 1H, lac.H), 5.72 (dd, $J = 2.4$, 8.5, 2H, lac.H), 5.55 (brs, 7 × lac.H and H_2O), 5.05 (d, $J = 7.0$, 1H, H-17), 4.56−4.68 (m, 2H, lac.H), 4.44−4.51 (m, 4H, $NCH_2(CH_2)_4CH_3$ and lac.H), 4.40−4.43 (m, 1H, lac.H), 4.34−4.38 (m, 1H, lac.H), 4.25−4.29 (m, 2H, H-18 and lac.H), 4.05−4.13 (m, 3H, lac.H), 4.00 (s, 3H, CH_3-12), 3.93−3.96 (m, 1H, lac.H), 3.73−3.79 (m, 4H, CH_2-3, CH_2-8), 3.23 (s, 3H, CH_3-2), 3.20 (s, 3H, CH_3-7), 3.03−3.16 (m, 1H, H-17^1), 2.90−3.00 (m, 1H, H-17^2), 2.75−2.83 (m, 1H, H-17^1), 2.45−2.57 (m, 1H, H-17^2), 2.01−2.14 (m, 2H, $NCH_2CH_2(CH_2)_3CH_3$), 1.79 (d, $J = 6.5$, 3H, CH_3-18), 1.68−1.75 (m, 6H, CH_3-3^1 and CH_3-8^1), 1.55−1.66 (m, 2H, $N(CH_2)_2CH_2(CH_2)_2CH_3$), 1.28−1.43 (m, 4H, $N(CH_2)_3(CH_2)_2$ CH_3), 0.87 (t, $J = 7.0$, 3H, $N(CH_2)_5$ CH_3), 0.37 (brs, 1H, NH), 0.17 (brs, 1H, NH). Mass (ESI): 995 ($M^+ + Na$).

Mesopurpurin−18-*N*-(3-Propargyllactose)benzylimide Conjugate (7). Yield: 80% (the product was purified by silica gel preparative TLC using 15% MeOH in CH_2Cl_2 as eluant). Mp: 280−282 °C. UV−vis (CH_2Cl_2): 695 (4.41×10^4), 641 (8.59×10^3), 545 (2.14×10^4), 508 (7.80×10^3), 418 (1.50×10^5), 362 (4.65×10^4). ^{1}H NMR (20% CD_3OD in $CDCl_3$, 400 MHz): δ 9.57 (s, 1H, mesoH-10), 9.18 (s, 1H, mesoH-5), 8.51 (s, 1H, mesoH-20), 7.77 (s, 1H, ArH), 7.68−7.70 (m, 1H, ArH), 7.32−7.35 (m, 2H, ArH), 5.64 (s, 2H, NCH_2), 5.31−5.34 (m, 1H, H-17), 4.53−4.66 (m, 2H, lac.H), 4.31−4.36 (m, 1H, 18H), 4.11 (brs, 7 × lac.OH), 3.82−3.87 (m, 3H, OCH_2 and lac.H), 3.71−3.81 (m, 4H, CH_2-3 and lac.H), 3.78 (s, 3H, CH_3-12), 3.55−3.69 (m, 8H, CH_2-8^1 and lac.H), 3.56 (s, 3H, CO_2CH_3-17^2), 3.35−3.38 (m, 3H, lac.H), 3.24 (s, 3H, CH_3-2), 3.17 (s, 3H, CH_3-7), 2.65−2.70 (m, 1H, H-17^1), 2.27−2.38 (m, 2H, 2 × H-17^2), 1.91−2.03 (m, 1H, H-17^2), 1.60−1.77 (m, 9H, CH_3-18, 3^2 and 8^2), 0.09 (brs, 2H, 2 × NH). Mass (ESI): 1070 ($M^+ + Na$).

Synthesis of 3^1-*O*-Glucose−Purpurin-18-*N*-hexylimide Conjugate (8). Yield: 90%. Mp: 196−200 °C. UV−vis (THF): 700 (6.06×10^4), 643 (7.92×10^3), 543 (2.25×10^4), 508 (8.23×10^3), 415 (1.58×10^5), 364 (5.42×10^4). ^{1}H NMR (pyridine-d_5, 400 MHz): δ 10.07 (s, 1H, mesoH-10), 9.92 (s, 1H, mesoH-5), 8.84 (s, 1H, mesoH-20), 6.36 (d, $J = 12.0$, 1H, H-3^1), 6.14 (d, $J = 12.4$, 1H, H-3^1), 5.70 (d, $J = 8.4$, 1H, H-17), 5.47 (d, $J = 7.2$, 1H, glu.H), 4.86 (d, $J = 10.0$, 1H, glu.H), 4.62−4.71 (m, 3H, $NCH_2(CH_2)_4CH_3$ and glu.H), 4.50 (q, $J = 7.6$, 1H, H-18), 4.29−4.45 (m, 3H, all glu.H), 4.24−4.28 (m, 1H, glu.H), 3.96 (s, 3H, CH_3-12), 3.64−3.72 (m, 2H, CH_2-8), 3.61 (s, 3H, CO_2CH_3-17^2), 3.36 (s, 3H, CH_3-2), 3.21 (s, 3H, CH_3-7), 3.03−3.07 (m, 1H, H-17^2), 2.78−2.84 (m, 2H, H-$17^1$and H-17^2), 2.26−2.31 (m, 1H, H-17^2), 2.10−2.17 (m, 2H, $NCH_2CH_2(CH_2)_3CH_3$), 1.82 (d, $J = 7.2$, 3H, CH_3-18), 1.66 (t, $J = 7.6$, 3H, CH_3-8^1), 1.56−1.62 (m, 2H, $N(CH_2)_2CH_2(CH_2)_2CH_3$), 1.28−1.42 (m, 4H, $N(CH_2)_3(CH_2)_2CH_3$), 0.88 (t, $J = 7.0$, 3H, $N(CH_2)_5CH_3$), 0.08 (brs, 1H, NH), 0.01 (brs, 1H, NH). Mass (ESI): 851.1 ($M^+ + H + Na$).

Synthesis of 3^1-*O*-Galactose−Purpurin-18-*N*-hexylimide Conjugate (9). Yield: 90%. Mp: 183−186 °C. UV−vis (THF): 700 (6.06×10^4), 642 (8.64×10^3), 543 (2.31×10^4), 507 8.75×10^3), 415 (1.58×10^5), 364 (5.53×10^4). ^{1}H NMR (pyridine-d_5, 400 MHz): δ 10.10 (s, 1H, mesoH-10), 9.98 s, 1H, mesoH-5), 8.84 (s, 1H, mesoH-20), 6.38 (d, $J = 12.0$, 1H, H-3^1), 6.16 (d, $J = 11.6$, 1H, H-3^1), 5.70 (d, $J = 8.4$, 1H, H-17), 5.55 (brs, 6H, all gal.OH), 5.40 (d, $J = 7.6$, 1H, gal.H), 4.66−4.81 (m, 6H, $NCH_2(CH_2)_4CH_3$ and gal.H), 4.50 (q, $J = 7.2$, 1H, H-18), 4.36 (t, $J = 6.0$, 1H, gal.H), 4.30 (dd, $J = 2.4$, 9.6, 1H, gal.H), 4.00 (s, 3H, CH_3-12), 3.70 (q, $J = 7.6$, 2H, CH_2-8), 3.61 (s, 3H, CO_2CH_3-17^2), 3.36 (s, 3H, CH_3-2), 3.23 (s, 3H, CH_3-7), 3.01−3.08 (m, 1H, H-17^2), 2.78−2.84 (m, 2H, H-$17^1$and H-17^2), 2.26−2.31 (m, 1H, H-17^2), 2.10−2.17 (m, 2H, $NCH_2CH_2(CH_2)_3CH_3$), 1.81 (d, $J = 6.8$, 3H, CH_3-18), 1.67 (t, $J = 7.6$, 3H, CH_3-8^1), 1.56−1.62 (p, $J = 7.2$, 2H, $N(CH_2)_2CH_2(CH_2)_2CH_3$), 1.28−1.42 (m, 4H, $N(CH_2)_3(CH_2)_2CH_3$), 0.87 (t, $J = 7.2$, 3H, $N(CH_2)_5CH_3$), 0.13 (brs, 1H, NH), 0.05 (brs, 1H, NH). Mass (ESI): 850.7 ($M^+ + Na$), 829.4 ($M^+ + 2H$).

Synthesis of 3^1-Hydroxypurpurin-18-*N*-hexylimide (13). To a solution of 3-formylpurpurin-18-*N*-hexylimide (**12**) (150 mg)[33] in CH_2Cl_2:MeOH (19:1 mL), sodium borohydride (20 mg) was added and the reaction mixture was stirred under N_2 at RT for 5 min. The reaction was quenched with 2% AcOH in H_2O (50 mL), diluted with CH_2Cl_2 (150 mL) and the separated organic layer was washed with H_2O (3 × 100 mL). The organic layer was dried over Na_2SO_4, concentrated, and purified over a silica column using 5% acetone in CH_2Cl_2 as eluant to afford 120 mg (80%) of the product **13**. Mp: 142−144 °C. UV−vis (CH_2Cl_2): 702 (6.06×10^4), 645 (1.01×10^4), 544 (2.50×10^5), 508 (1.11×10^4), 416 (1.83×10^5), 366 (6.31×10^4). ^{1}H NMR ($CDCl_3$, 400 MHz): δ 9.64 (s, 1H, mesoH-10), 9.48 (s, 1H, mesoH-5), 8.61 (s, 1H, mesoH-20), 5.86 (s, 2H, CH_2-3), 5.39−5.46 (dd, $J = 3.2$, 9.8, 1H, H-17), 4.44−4.54 (m, 2H, $NCH_2(CH_2)_4CH_3$), 4.38 (q, $J = 7.3$, 1H, H-18), 3.84 (s, 3H, CH_3-12), 3.68 (q, $J = 7.3$, 2H, CH_2-8), 3.58 (s, 3H, CO_2CH_3-17^2), 3.39 (s, 3H, CH_3-2), 3.21 (s, 3H, CH_3-7), 2.65−2.76 (m, 1H, H-17^1), 2.31−2.50 (m, 2H, H-17^2 and H-17^1), 1.94−2.08 (m, 3H, H-17^2 and $NCH_2CH_2(CH_2)_3CH_3$), 1.78 (d, $J = 6.6$, 3H, CH_3-18), 1.69 (t, $J = 7.6$, 3H, CH_3-8^1), 1.64 (p, $J = 7.6$, 2H, $N(CH_2)_2CH_2(CH_2)_2CH_3$), 1.40−1.53 (m, 4H, $N(CH_2)_3(CH_2)_2CH_3$), 0.97 (t, $J = 7.1$, 3H, $N(CH_2)_5CH_3$), −0.25 (brs, 1H, NH), −0.28 (brs, 1H, NH). Mass (ESI): 688 ($M^+ + Na$), 666 (MH^+). Similarly compound 8^1-hydroxypurpurin-18-*N*-hexylimide (**18**) was synthesized starting with 8-formylpurpurin-18-*N*-hexylimide (**17**).[33]

8^1-Hydroxypurpurin-18-*N*-hexylimide (18). Yield: 80% Mp: 150−52 °C UV−vis (CH_2Cl_2): 689 (2.81×10^4), 634 (4.39×10^3), 545 (1.01×10^4), 508 (5.84×10^3), 419 (1.12×10^5), 363 (2.48×10^4). ^{1}H NMR ($CDCl_3$, 400 MHz): δ 9.84 (s, 1H, mesoH-10), 9.22 (s, 1H, mesoH-5), 8.55 (s, 1H, mesoH-20), 5.73 (s, 2H, CH_2-8), 5.40−5.43 (m, 1H, H-17), 4.44−4.49 (m, 2H, NCH_2(CH_2)$_4$$CH_3$), 4.36 (q, J = 6.9, 1H, H-18), 3.81 (s, 3H, CH_3-12), 3.76−3.82 (m, 2H, CH_2-3), 3.59 (s, 3H, CO_2CH_3-17^2), 3.31 (s, 3H, CH_3-2), 3.28 (s, 3H, CH_3-7), 2.66−2.74 (m, 1H, H-17^1), 2.35−2.48 (m, 2H, H-17^2 and H-17^1), 1.94−2.04 (m, 3H, H-17^2 and $NCH_2CH_2(CH_2)_3CH_3$), 1.78 (d, J = 7.1, 3H, CH_3-18), 1.74 (t, J = 7.6, 3H, CH_3-3^1), 1.37−1.67 (m, 6H, N(CH_2)$_2$(CH_2)$_3$$CH_3$), 0.97 (t, J = 7.2, 3H, N(CH_2)$_5$CH_3), −0.02 (brs, 1H, NH), −0.17 (brs, 1H, NH). Mass (ESI): 688 (M^+ + Na).

Synthesis of 17^2-Carboxylmesopurpurin-18-*N*-hexylpurpurinimide (19). Aqueous LiOH (200 mg in 10 mL of H_2O) was added to a solution of mesopurpurin-18-*N*-hexylimide **14** (150 mg) in dry THF:MeOH (15: 10 mL), and the reaction mixture was stirred under argon at RT for 1.5 h. The reaction mixture was diluted with CH_2Cl_2 (300 mL) and washed with 2% AcOH in H_2O (100 mL) and with H_2O (3 × 200 mL), and the organic layer was dried over Na_2SO_4, concentrated, and purified over a preparative TLC plate using 5% MeOH in CH_2Cl_2 as eluant to yield 100 mg (70%) of product **19** and 25 mg of 17^2-carboxylic acid derivative of compound **20**. Mp: 228−32 °C. UV−vis (CH_2Cl_2): 694 (4.76×10^4), 641 (8.90×10^3), 545 (2.12×10^4), 508 (8.40×10^3), 479 (4.88×10^3), 417 (1.56×10^5), 363 (5.28×10^4), 310 (1.87×10^4). ^{1}H NMR ($CDCl_3$, 400 MHz): δ 9.52 (s, 1H, mesoH-10), 9.13 (s, 1H, mesoH-5), 8.44 (s, 1H, mesoH-20), 5.33 (d, J = 7.3, 1H, H-17), 4.35−4.48 (m, 2H, NCH_2(CH_2)$_4$$CH_3$), 4.30 (q, J = 7.6, 1H, H-18), 3.76 (s, 3H, CH_3-12), 3.64−3.72 (m, 2H, CH_2-8), 3.60 (q, J = 7.7, 2H, CH_2-3), 3.11−3.22 (brs, 6H, CH_3− 2 and 7), 2.65−2.81 (m, 1H, H-17^1), 2.31−2.50 (m, 2H, H-17^2 and H-17^1), 1.83−2.06 (m, 3H, H-17^2 and $NCH_2CH_2(CH_2)_3CH_3$), 1.70 (d, J = 6.5, 3H, CH_3-18), 1.60−1.68 (m, 6H, CH_3-8^1- and CH_3-3^1), 1.51−1.60 (m, 2H, N(CH_2)$_2$CH_2(CH_2)$_2$$CH_3$), 1.31−1.47 (m, 4H, N($CH_2$)$_3$(C$H_2$)$_2$$CH_3$), 0.89 (t, J = 7.1, 3H, N(CH_2)$_5$CH_3), −0.06 (brs, 1H, NH), −0.30 (brs, 1H, NH). Mass (ESI): 672 (M^+ + Na), 650 (MH^+).

Synthesis of 12^1-Hydroxypurpurin-18-*N*-hexylpurpurinimide (23). Aqueous LiOH (200 mg in 10 mL of H_2O) was added to a solution of mesopurpurin-18-*N*-hexylimide **14** (150 mg) in THF:MeOH (15:10 mL), and the reaction mixture was stirred at RT overnight (16 h) in air. It was then diluted with CH_2Cl_2 (300 mL) and washed with 2% AcOH in H_2O (100 mL) and with H_2O (3 × 200 mL), and the organic layer was dried over Na_2SO_4 and concentrated to dryness. The product was treated with CH_2N_2 and purified over a preparative silica gel TLC plate using 2% acetone in CH_2Cl_2 as eluant to yield 105 mg (70%) of product **23**. Mp: 170−75 °C UV−vis (CH_2Cl_2): 694 (3.77×10^4), 638 (9.03×10^3), 549 (2.18×10^4), 512 (6.10×10^3), 481 (4.24×10^3), 417 (1.17×10^5), 364 (4.58×10^4), 311 (1.73×10^4).^{1}H NMR ($CDCl_3$, 400 MHz): δ 9.46 (s, 1H, mesoH-10), 9.01 (s, 1H, mesoH-5), 8.39 (s, 1H, mesoH-20), 6.16 (t, J = 6.5, 1H, OH-12^1), 5.98−6.08 (m, 2H, CH_2-12), 5.27−5.35 (m, 1H, H-17), 4.41−4.51 (m, 2H, NCH_2(CH_2)$_4$$CH_3$), 4.29 (q, J = 7.6, 1H, H-18), 3.67 (q, J = 7.6, 2H, CH_2-3), 3.57 (s, 3H, CO_2CH_3-17^2), 3.51−3.60 (m, 2H, CH_2-8), 3.18 (s, 3H, CH_3-2), 3.09 (s, 3H, CH_3-7), 2.63−2.75 (m, 1H, H-17^1), 2.31−2.47 (m, 2H, H-17^2 and H-17^1), 1.92−2.06 (m, 3H, 17^{2}H and $NCH_2CH_2(CH_2)_3CH_3$), 1.74 (d, J = 7.6, 3H, CH_3-18), 1.66 (t, J = 7.6, 3H, CH_3-8^1), 1.62 (t, J = 7.6, 3H, CH_3-3^1), 1.56−1.59 (m, 2H, N(CH_2)$_2$CH_2(CH_2)$_2$$CH_3$), 1.36−1.52 (m, 4H, N($CH_2$)$_3$(C$H_2$)$_2$$CH_3$), 0.95 (t, J = 7.1, 3H, N(CH_2)$_5$CH_3), 0.58 (brs, 1H, NH), 0.29 (brs, 1H, NH). Mass (ESI): 702 (M^+ + Na).

Synthesis of Mesopurpurin-18-*N*-(3-iodobenzyl)imide (25). Mesopurpurin-18-methyl ester **24**[32] (200 mg) and 3-iodobenzyl amine (0.5 mL, a large excess) were refluxed in benzene (10 mL) for 36 h under a nitrogen atmosphere. The reaction was monitored periodically by UV−vis spectroscopy, and the absence of a peak at 687 nm (for the anhydride) and the appearance of a new peak at 695 nm (for the purpurinimide) indicated completion of the reaction. The crude material obtained after evaporating the solvents from the reaction mixture was purified over a silica gel column using 2% acetone in CH_2Cl_2 as eluant to yield 170 mg (85%) of pure product **25**. Mp: 177−80 °C. UV−vis (CH_2Cl_2): 695 (4.41×10^4), 642 (8.45×10^3), 545 (7.88×10^3), 508 (7.88×10^3), 482 (4.47×10^3), 418 (1.48×10^5), 363 (4.64×10^4). ^{1}H NMR ($CDCl_3$, 400 MHz): δ 9.59 (s, 1H, mesoH-10), 9.19 (s, 1H, mesoH-5), 8.49 (s, 1H, mesoH-20), 8.09 (s, 1H, ArH), 7.71 (d, J = 7.5, 1H, ArH), 7.61 (d, J = 7.2, 1H, ArH), 7.11 (t, J = 7.8, 1H, ArH), 5.63 (s, 2H, benzylic CH_2), 5.33−5.39 (m, 1H, H-17), 4.33 (q, J = 6.9, 1H, H-18), 3.81 (s, 3H, CH_3-12), 3.76 (q, J = 7.7, 2H, CH_2-3), 3.64 (q, J = 7.7, 2H, CH_2-8), 3.57 (s, 3H, CO_2CH_3-17^2), 3.24 (s, 3H, CH_3-2), 3.18 (s, 3H, CH_3-7), 2.64−2.72 (m, 1H, H-17^1), 2.34−2.42 (m, 2H, H-17^2 and H-17^1), 1.92−2.02 (m, 3H, H-17^2), 1.76 (d, J = 8.3, 3H, CH_3-18), 1.71 (t, J = 6.8, 3H, CH_3-3^1), 1.67 (t, J = 7.6, 3H, CH_3-8^1), 0.15 (brs, 1H, NH), −0.05 (brs, 1H, NH). Mass (ESI): 796 (MH^+), 818 (M^+ + Na).

Following the synthetic approach similar to that for conjugate **26**, compounds 3^1-*O*-tetraacetoglucose−purpurin-18-*N*-hexylimide conjugate **31** and 3^1-*O*-tetraacetogalactose−purpurin-18-*N*-hexylimide conjugate **32** were synthesized starting from 3^1-hydroxypurpurin-18-*N*-hexylimide **13**.

Synthesis of 3^1-*O*-Heptaacetolactose−Purpurin-18-*N*-hexylimide Conjugate (26). BF_3·Et_2O (120 μL) was added to a cold solution (−10 °C) of 3^1-hydroxypurpurin-18-*N*-hexylimide (**13**) (60 mg) and lactose octaacetate (100 mg) in dry CH_2Cl_2 (5 mL). The reaction mixture was stirred for 4 h under a nitrogen atmosphere. During this time the temperature was gradually raised to room temperature (25 °C). The reaction mixture was then diluted with CH_2Cl_2 (50 mL) and washed with a saturated solution of $NaHCO_3$ (2 × 50 mL). The combined $NaHCO_3$ layer was washed with CH_2Cl_2 (25 mL). The combined organic layer was washed with H_2O (2 × 50 mL), dried over Na_2SO_4, concentrated under

reduced pressure, and purified over silica gel preparative TLC plates using 5% acetone in CH_2Cl_2 as eluant. Two bands were collected. A fast moving band isolated in a 10 mg quantity was found to be the starting material, while the slow moving band isolated in an 80 mg quantity (83%) was the desired product **26**. Mp: 131−134 °C. UV−vis (CH_2Cl_2): 704 (6.06×10^4), 648 (8.46×10^3), 545 (2.31×10^4), 508 (9.01×10^3), 416 (1.71×10^5), 366 (5.92×10^4). ^{1}H NMR ($CDCl_3$, 400 MHz): δ 9.67 (s, 1H, mesoH-10), 9.36 (s, 1H, mesoH-5), 8.64 (s, 1H, mesoH-20), 6.01 (d, J = 12.5, 1H, H-3^1), 5.84 (d, J = 12.6, 1H, H-3^1), 5.45 (dd, J = 2.9, 8.5, 1H, H-17), 5.33 (d, J = 3.7, 1H, lac.H), 4.94−5.09 (m, 4H, lac.H), 4.69−4.75 (m, 2H, lac.H), 4.45−4.52 (m, 3H, NCH_2(CH$_2$)$_4$CH$_3$ and lac.H), 4.40 (q, J = 7.0, 1H, H-18), 4.21 (dd, J = 4.9,11.9, 1H, lac.H), 4.01−4.12 (m, 2H, lac.H), 3.84−3.91 (m, 2H, lac.H), 3.86 (s, 3H, CH$_3$-12), 3.63−3.71 (m, 3H, CH$_2$-8 and lac.H), 3.58 (s, 3H, CO$_2$CH$_3$-17^2), 3.36 (s, 3H, CH$_3$-2), 3.20 (s, 3H, CH$_3$-7), 2.68−2.75 (m, 1H, H-17^2), 2.41−2.49 (m,1H, H-17^1), 2.32−2.39 (m, 1H, H-17^2), 2.24 (s, 3H, COCH$_3$ of lac.), 2.11 (s, 3H, COCH$_3$ of lac.), 2.04−2.07 (m, 1H, H-17^1), 2.05 (s, 3H, COCH$_3$ of lac.), 1.98−2.02 (m, 2H, NCH$_2$CH_2(CH$_2$)$_3$CH$_3$), 2.02 (s, 3H, COCH$_3$ of lac.), 1.97 (s, 3H, COCH$_3$ of lac.), 1.95 (s, 3H, COCH$_3$ of lac.), 1.79 (d, J = 7.6, 3H, CH$_3$-18), 1.68 (t, J = 7.6, 3H, CH$_3$-8^1), 1.59−1.65 (m, 2H, N(CH$_2$)$_2$CH_2(CH$_2$)$_2$-CH$_3$), 1.44−1.52 (m, 4H, N(CH$_2$)$_3$(CH_2)$_2$CH$_3$), 1.42 (s, 3H, COCH$_3$ of lac.), 0.96 (t, J = 6.8, 3H, N(CH$_2$)$_5$CH_3), −0.30 (brs, 2H, 2 × NH). Mass (ESI**)**: 1306 (M^+ + Na), 1284 (M^+).

Following a similar synthetic approach, compounds 8^1-*O*-heptaacetolactose−purpurin-18-*N*-hexylimide (**27**) and 12^1-O-heptaacetolactose−purpurin-18-*N*-hexylimide conjugate (**28**) were synthesized from their corresponding starting materials 8^1-hydroxypurpurin-18-*N*-hexylimide (**18**) and 12^1-hydroxypurpurin-18-*N*-hexylpurpurin-imide (**23**) respectively.

8^1-*O*-Heptaacetolactose−Purpurin-18-*N*-hexylimide Conjugate (27). Yield: 90%. Mp: 128−31 °C. UV−vis (CH_2Cl_2): 688 (2.81×10^4), 634 (4.23×10^3), 545 (9.20×10^3), 509 (5.95×10^3), 420 (1.11×10^5), 365 (2.27×10^4), 310 (1.11×10^4). ^{1}H NMR ($CDCl_3$, 400 MHz): δ 9.63 (s, 1H, mesoH-10), 9.23 (s, 1H, mesoH-5), 8.54 (s, 1H, mesoH-20), 5.87 (d, J = 11.8, 1H, H-8^1), 5.65 (d, J = 12.7, 1H, H-8^1), 5.37−5.41 (m, 1H, H-17), 5.31 (d, J = 3.2, 1H, lac.H), 5.00−5.07 (m, 2H, lac.H), 4.91−4.98 (m, 2H, lac.H), 4.65−4.72 (m, 2H, lac.H) 4.40−4.50 (m, 3H, NCH_2(CH$_2$)$_4$CH$_3$ and lac.H), 4.35 (q, J = 6.9, 1H, H-18), 4.20 (dd, J = 5.8, 12.2, 1H, lac.H), 3.98−4.07 (m, 2H, lac.H), 3.74−3.89 (m, 4H, CH$_2$-3 and lac.H), 3.77 (s, 3H, CH$_3$-12), 3.59−3.65 (m, 1H, lac.H), 3.56 (s, 3H, CO$_2$CH$_3$-17^2), 3.25 (s, 3H, CH$_3$-2), 3.24 (s, 3H, CH$_3$-7), 2.65−2.73 (m, 1H, H-17^1), 2.30−2.48 (m, 2H, H-17^2 and H-17^1), 2.25 (s, 3H, COCH$_3$ of lac.), 2.04−2.16 (m, 1H, H-17^2), 2.08 (s, 3H, COCH$_3$ of lac.), 2.04 (s, 3H, COCH$_3$ of lac.), 1.94−2.00 (m, 2H, NCH$_2$CH_2(CH$_2$)$_3$-CH$_3$), 1.99 (s, 3H, COCH$_3$ of lac.), 1.94 (s, 3H, COCH$_3$ of lac.), 1.90 (s, 3H, COCH$_3$ of lac.), 1.70−1.78 (m, 6H, CH$_3$-18 and CH$_3$-3^1), 1.57−1.68 (m, 2H, N(CH$_2$)$_2$CH_2(CH$_2$)$_2$CH$_3$), 1.38−1.51 (m, 4H, N(CH$_2$)$_3$(CH_2)$_2$CH$_3$), 1.24 (s, 3H, COCH$_3$ of lac.), 0.94 (t, J = 7.1, 3H, N(CH$_2$)$_5$CH_3), −0.08 (brs, 1H, NH), −0.21 (brs, 1H, NH). Mass (ESI): 1306 (M^+ + Na), 1284 (M^+).

12^1-*O*-Heptaacetolactose−Purpurin-18-*N*-hexylimide Conjugate (28). Yield: 70%. Mp: 132−35 °C (dec). UV−vis (CH_2Cl_2): 694 (3.77×10^4), 637 (8.67×10^4), 549 (1.92×10^4), 512 (6.62×10^3), 481 (4.17×10^3), 419 (1.11×10^5), 365 (4.23×10^4), 310 (1.73×10^4).^{1}H NMR ($CDCl_3$, 400 MHz): δ 9.69 (s, 1H, mesoH-10), 9.06 (s, 1H, mesoH-5), 8.42 (s, 1H, mesoH-20), 6.62 (d, J = 13.3, 1H, H-12^1), 6.29 (d, J = 12.8, 1H, H-12^1), 5.31−5.33 (m, 2H, H-17 and lac.H), 4.92−5.11 (m, 5H, lac.H), 4.67 (d, J = 10.7, 1H, lac.H), 4.48 (d, J = 7.6, 1H, lac.), 4.38−4.46 (m, 2H, NCH_2(CH$_2$)$_4$CH$_3$), 4.30 (q, J = 6.7, 1H, H-18), 4.22 (dd, J = 5.8, 12.1, 1H, lac.H), 4.00−4.15 (m, 2H, lac.H), 3.85 (q, J = 8.0, 2H, lac.H), 3.75 (dd, J = 3.2, 9.3, 1H, lac.), 3.71 (q, J = 7.7, 2H, CH$_2$-3), 3.56−3.63 (m, 2H, CH$_2$-8), 3.56 (s, 3H, CO$_2$CH$_3$-17^2), 3.20 (s, 3H, CH$_3$-2), 3.13 (s, 3H, CH$_3$-7), 2.67−2.71 (m, 1H, H-17^1), 2.34−2.43 (m, 1H, H-17^2 and H-17^1), 2.16 (s, 3H, COCH$_3$ of lac.), 2.11 (s, 3H, COCH$_3$ of lac.), 2.08 (s, 3H, COCH$_3$ of lac.), 2.02 (s, 3H, COCH$_3$ of lac.), 1.96 (s, 3H, COCH$_3$ of lac.), 1.96−2.04 (m, 3H, H-17^2 and NCH$_2$CH$_2$(CH$_2$)$_3$CH$_3$), 1.89 (s, 3H, COCH$_3$ of lac.), 1.74 (d, J = 7.4, 3H, CH$_3$-18), 1.57−1.71 (m, 8H, CH$_3$-3,^{1} CH$_3$-8^1 and N(CH$_2$)$_2$CH$_2$(CH$_2$)$_2$CH$_3$), 1.39−1.52 (m, 4H, N(CH$_2$)$_3$-(CH$_2$)$_2$CH$_3$), 0.95 (t, J = 7.2, 3H, N(CH$_2$)$_5$CH$_3$), 0.83 (s, 3H, COCH$_3$ of lac.), 0.52 (brs, 1H, NH), 0.18 (brs, 1H, NH). Mass (ESI): 1320 (M^+ + Na), 1298 (M^+).

Synthesis of 17^2-Aminoacylheptaacetolactose−Mesopurpurin-18-*N*-hexylimide Conjugate (29). BOP (70 mg) was added to a solution of 1-aminoheptaacetolactose (150 mg) and mesopurpurin-17-propionicacid-18-*N*-hexylimide (**19**) (80 mg) in dry CH_2Cl_2 (5 mL) containing triethylamine (0.2 mL), and the reaction mixture was stirred at room temperature under a nitrogen atmosphere for 2 h. The reaction mixture was then diluted with CH_2Cl_2 (50 mL), washed with H_2O (3 × 100 mL), dried over Na_2SO_4, concentrated, and purified over silica gel preparative TLC plates using 4% MeOH in CH_2Cl_2 as eluant to yield 70 mg (45%) of product **25**. Mp: 230−32 °C. UV−vis (CH_2Cl_2): 694 (4.76×10^4), 639 (8.23×10^3), 544 (2.13×10^4), 508 (8.31×10^3), 479 (4.53×10^3), 418 (1.55×10^5), 362 (4.86×10^4), 310 (1.66×10^4). ^{1}H NMR ($CDCl_3$, 400 MHz): δ 9.59 (s, 1H, mesoH-10), 9.19 (s, 1H, mesoH-5), 8.48 (s, 1H, mesoH-20), 7.33 (d, J = 9.7, 1H, CONH), 5.27−5.36 (m, 2H, 17H and lac.H), 5.20−5.25 (m, 1H, lac.H), 5.06−5.12 (m, 1H, lac.H), 5.00 (t, J = 9.7, 1H, lac.H), 4.94 (dd, J = 3.8, 9.5, 1H, lac.H), 4.45−4.52 (m, 4H, NCH$_2$(CH$_2$)$_4$CH$_3$ and lac.H), 4.38 (d, J = 12.4, 1H, lac.H), 4.32 (q, J = 6.7, 1H, H-18), 4.04−4.15 (m, 3H, lac.H), 3.80−3.86 (m, 1H, lac.H), 3.80 (s, 3H, CH$_3$-12), 3.70−3.78 (m, 3H, 3CH$_2$ and lac.H), 3.64 (q, J = 7.8, 2H, CH$_2$-8) 3.44−3.50 (m, 1H, lac.H) 3.24 (s, 3H, CH$_3$-2), 3.17 (s, 3H, CH$_3$-7), 2.67−2.74 (m, 1H, H-17^1), 2.40−2.46 (m, 1H, H-17^2), 2.29−2.37 (m, 1H, H-17^1), 2.15 (s, 3H, COCH$_3$ of lac.), 2.00−2.08 (m, 13H, 4 × COCH$_3$ of lac. and H-17^2), 1.90−1.98 (m, 8H, 2 x COCH$_3$ of lac. and NCH$_2$-

$CH_2(CH_2)_3CH_3$), 1.63−1.72 (m, 9H, $18CH_3$, CH_3-3^1 and CH_3-8^1), 1.57−1.62 (m, 2H, $N(CH_2)_2CH_2(CH_2)_2CH_3$), 1.25−1.52 (m, 4H, $N(CH_2)_3(CH_2)_2CH_3$), 0.96 (t, J = 7.0, 3H, $N(CH_2)_5CH_3$), 0.08 (brs, 1H, NH), −0.08 (brs, 1H, NH). Mass (ESI): 1289 (M^+ + Na), 1267 (M^+).

Synthesis of Mesopurpurin−18-*N*-{(3-Propargylhepta-acetolactose)benzyl}imide Conjugate (30). Triphenylarsine (7 mg) and Pd_2dba_3 (10 mg) were added to a stirred solution of mesopurpurin-18-*N*-(3-iodo)benzylimide (**25**) (25 mg) and propargyllactose heptaacetate (30 mg) in dry THF (30 mL) and dry Et_3N (4 mL). The reaction mixture was stirred at room temperature under an argon atmosphere overnight. As per TLC only half the amount of the starting purpurin reacted to produce the desired product. The remaining half was unreacted even by increasing the catalyst quantity, temperature, or duration of the reaction. The product (**30**) (18 mg) and the remaining starting purpurin (10 mg) were purified by preparative TLC plates using 3% MeOH in CH_2Cl_2 as eluant. Yield: 18 mg (72%). Mp: 126−128 °C (dec). UV−vis (CH_2Cl_2): 694 (4.41×10^4), 639 (7.80×10^3), 545 (2.05×10^4), 508 (7.31×10^3), 478 (4.05×10^3), 417 (1.44×10^5), 362 (4.40×10^4). ^{1}H NMR ($CDCl_3$, 400 MHz): δ 9.61 (s, 1H, mesoH-10), 9.21 (s, 1H, mesoH-5), 8.50 (s, 1H, mesoH-20), 7.82 (s, 1H, ArH), 7.74−7.76 (m, 1H, ArH), 7.33−7.36 (m, 2H, ArH), 5.67 (s, 2H, NCH_2), 5.34−5.39 (m, 2H, H-17 and lac.H), 5.24 (t, J = 8.9, 1H, lac.H), 5.08−5.13 (m, 1H, lac.H), 4.91−5.00 (m, 2H, lac.H), 4.82−4.85 (m, 1H, lac.H), 4.48−4.58 (m, 4H, OCH_2 and lac.H), 4.33 (q, J = 7.4, 1H, H-18), 4.08−4.15 (m, 3H, lac.H), 3.74−3.90 (m, 4H, lac.H and CH_2-3^1), 3.83 (s, 3H, CH_3-12), 3.64−3.70 (m, 3H, CH_2-8^1 and lac.H), 3.56 (s, 3H, CO_2CH_3-17^2), 3.25 (s, 3H, CH_3-2), 3.19 (s, 3H, CH_3-7), 2.63−3.00 (m, 1H, H-17^2), 2.30−2.41 (m, 2H, 2 × H-17^1), 1.95−2.18 (m, 22H, 7 x $COCH_3$ and H-17^2), 1.76 (d, J = 7.8, 3H, CH_3-18), 1.67−1.74 (m, 6H, CH_3-3^2 and 8^2), 0.15 (brs, 1H, NH), −0.05 (brs, 1H, NH). Mass (ESI): 1341 (M^+).

General Procedure for the Deacetylation of Heptaacetolactose−Purpurin Conjugates (26−30). 1 M NaOMe in MeOH (150 μL) was added to a solution of 3^1-*O*-heptaacetolactose−purpurin-18-*N*-hexylimide (**26**) (45 mg) in dry CH_2Cl_2 (5 mL) and dry MeOH (2 mL), and the reaction mixture was stirred under a nitrogen atmosphere for 30 min. AcOH (30 μL) was added, and the reaction mixture was diluted with CH_2Cl_2 (30 mL) and washed with H_2O (2 × 30 mL). The CH_2Cl_2 layer was dried over Na_2SO_4 and concentrated, and the crude compound thus obtained was purified over silica gel preparative TLC plates using 15% MeOH in CH_2Cl_2 as eluant to yield 26 mg of pure product 3^1-*O*-lactose−purpurin-18-*N*-hexylimide conjugate (**3**). Yield: 26 mg (75%). Mp: 242−244 °C. UV−vis (THF): 700 (6.06×10^4), 642 (8.50×10^3), 543 (2.18×10^4), 507 (8.39×10^3), 415 (1.55×10^5), 364 (5.49×10^4). ^{1}H NMR (pyridine-d_5, 400 MHz**)**: δ 10.00 (s, 1H, mesoH-10), 9.99 (s, 1H, mesoH-5), 8.83 (s, 1H, mesoH-20), 6.90 (brs, 1H, lac.OH), 6.58 (brs, 2H, lac.OH), 6.54 (brs, 1H, lac.OH), 6.32 (d, J = 12.4, 1H, H-3^1), 6.21 (brs, 1H, lac.OH), 6.12 (d, J = 11.7, 1H, H-3^1), 5.70 (d, J = 9.8, 1H, H-17), 5.39 (d, J = 7.6, 1H, lac.H), 5.18 (d, J = 7.8, 1H, lac.H), 4.74−4.81 (m, 2H, lac.H), 4.66−4.72 (m, 2H, $NCH_2(CH_2)_4CH_3$), 4.58 (t, J = 8.7, 1H, lac.H), 4.45−4.55 (m, 3H, H-18 and lac.H), 4.40−4.46 (m, 2H, lac.H), 4.33−4.39 (m, 1H, lac.H), 4.26−4.32 (m, 1H, lac.H), 4.16−4.22 (m, 2H, lac.H), 4.10−4.16 (m, 1H, lac.H), 4.01 (s, 3H, CH_3-12), 3.73 (q, J = 7.3, 2H, CH_2-8) 3.60 (s, 3H, CO_2CH_3-17^2), 3.34 (s, 3H, CH_3-2), 3.23 (s, 3H, CH_3-7), 2.98−3.08 (m, 1H, H-17^1), 2.74−2.86 (m, 2H, H-17^2 and H-17^1), 2.24−2.34 (m, 1H, H-17^2), 2.10−2.20 (m, 2H, NCH_2 (CH_2)$(CH_2)_3CH_3$), 1.81 (d, J = 6.5, 3H, CH_3-18), 1.69 (t, J = 7.8, 3H, CH_3-8^1), 1.55−1.65 (m, 2H, $N(CH_2)_2(CH_2)(CH_2)_2CH_3$), 1.26−1.44 (m, 4H, $N(CH_2)_3(CH_2)_2CH_3$), 0.88 (t, J = 7.2, 3H, $N(CH_2)_5CH_3$), 0.13 (brs, 1H, NH), 0.04 (brs, 1H, NH). Mass (ESI): 1012 (M^+ + Na), 990 (M^+).

Synthesis of 3^1-*O*-Tetraacetoglucose−Purpurin-18-*N*-hexylimide Conjugate (31). Yield: 80%. Mp: 89−92 °C. UV−vis (CH_2Cl_2): 705 (6.06×10^4), 545 (2.36×10^4), 507 (9.90×10^3), 416 1.72×10^5), 365 (6.09×10^4). ^{1}H NMR ($CDCl_3$, 400 MHz): δ 9.67 (s, 1H, mesoH-10), 9.36 (s, 1H, mesoH-5), 8.63 (s, 1H, mesoH-20), 6.03 (d, J = 13.2, 1H, H-3^1), 5.88 (d, J = 12.8, 1H, H-3^1), 5.45 (dd, J = 2.2, 8.2, 1H, H-17), 5.14−5.20 (m, 2H, glu.H), 4.99 (t, J = 9.6, 1H, glu.H), 4.69 (d, J = 8.4, 1H, lac.H), 4.45−4.49 (m, 2H, H-18 and glu.H), 4.37−4.43 (m, 3H, $NCH_2(CH_2)_4CH_3$ and glu.H), 3.85 (s, 3H, CH_3-12), 3.64−3.74 (m, 3H, CH_2-8 and glu.H), 3.58 (s, 3H, CO_2CH_3-17^2), 3.36 (s, 3H, CH_3-2), 3.20 (s, 3H, CH_3-7), 2.68−2.75 (m, 1H, H-17^2), 2.31−2.49 (m, 2H, H-$17^1$and H-17^2), 2.19 (s, 3H, $COCH_3$ of glu.), 2.00−2.07 (m, 3H, H-17^1 and $NCH_2CH_2(CH_2)_3CH_3$), 1.98 (s, 3H, $COCH_3$ of glu.), 1.90 (s, 3H, $COCH_3$ of glu.), 1.79 (d, J = 7.2, 3H, CH_3-18), 1.68 (t, J = 7.6, 3H, CH_3-8^1), 1.59−1.65 (m, 2H, $N(CH_2)_2CH_2(CH_2)_2CH_3$), 1.43−1.52 (m, 4H, $N(CH_2)_3(CH_2)_2CH_3$), 1.41 (s, 3H, $COCH_3$ of glu.), 0.95 (t, J = 7.0, 3H, $N(CH_2)_5CH_3$), −0.30 (brs, 2H, 2 × NH). Mass (ESI): 1018.6 (M^+ + Na), 995.4 (M^+).

Synthesis of 3^1-*O*-Tetraacetogalactose−Purpurin-18-*N*-hexylimide Conjugate (32). Yield: 75%. Mp: 76−80 °C. UV−vis (CH_2Cl_2): 705 (6.06×10^4), 545 (2.41×10^4), 507 (1.07×10^4), 416 (1.73×10^5), 365 (6.19×10^4). ^{1}H NMR ($CDCl_3$, 400 MHz): δ 9.69 (s, 1H, mesoH-10), 9.39 (s, 1H, mesoH-5), 8.63 (s, 1H, mesoH-20), 6.05 (d, J = 12.8, 1H, H-3^1), 5.88 (d, J = 12.8, 1H, H-3^1), 5.44 (dd, J = 2.8, 8.8, 1H, H-17), 5.34−5.40 (m, 2H, gal.H), 4.83 (dd, J = 3.2, 10.0, 1H, gal.H), 4.68 (d, J = 8.0, 1H, H-18 and gal.H), 4.44−4.50 (m, 2H, H-18 and gal.H), 4.38−4.43 (m, 2H, $NCH_2(CH_2)_4CH_3$), 4.29−4.34 (m, 1H, gal.H), 3.97 (t, J = 6.6, 1H, gal.H), 3.86 (s, 3H, CH_3-12), 3.66−3.73 (m, 2H, CH_2-8), 3.58 (s, 3H, CO_2CH_3-17^2), 3.37 (s, 3H, CH_3-2), 3.21 (s, 3H, CH_3-7), 2.68−2.75 (m, 1H, H-17^2), 2.28−2.48 (m, 2H, H-$17^1$and H-17^2), 2.21 (s, 3H, $COCH_3$ of gal.), 2.13 (s, 3H, $COCH_3$ of gal.), 1.96−2.04 (m, 3H, H-17^1 and $NCH_2CH_2(CH_2)_3CH_3$), 1.98 (s, 3H, $COCH_3$ of gal.), 1.88 (s, 3H, $COCH_3$ of gal.), 1.77 (d, J = 6.8, 3H, CH_3-18), 1.69 (t, J = 7.6, 3H, CH_3-8^1), 1.57−1.65 (m, 2H, $N(CH_2)_2CH_2(CH_2)_2CH_3$), 1.40−1.48 (m, 4H, $N(CH_2)_3(CH_2)_2CH_3$), 1.37 (s, 3H,

$COCH_3$ of glu.), 0.96 (t, $J = 7.0$, 3H, $N(CH_2)_5CH_3$), −0.28 (brs, 2H, 2 × NH). Mass (ESI): 1018.6 ($M^+ + Na$), 995.4 (M^+).

MTT Assay for *in Vitro* Photosensitizing Activity. The photosensitizing activity of conjugates (**1**−**9**) and **13** was determined in the RIF tumor cell line. The cells were grown in α-MEM with 10% fetal calf serum, L-glutamine, penicillin, and streptomycin. Cells were maintained in 5% CO_2, 95% air, and 100% humidity. Cells were plated in 96-well plates at a density of 5×10^3 cells per well in complete medium. After an overnight incubation at 37 °C, the photosensitizers were added at varying concentrations and incubated at 37 °C for 3 or 24 h in the dark. Prior to light treatment the cells were replaced with drug-free complete medium. Cells were then illuminated with an argon-pumped dye laser set at 700 nm at a dose rate of 3.2 mW/cm^2 for 0.5 or 1.0 J/cm^2. After PDT, the cells were incubated for 48 h at 37 °C in the dark. Following the 48 h incubation, 10 μL of 4.0 mg/mL solution of 3-[4,5-dimethylthiazol-2-yl]-2,5-diphenyltetrazoliumbromide (MTT) (Sigma, St. Louis, MO) dissolved in PBS was added to each well. After a 4 h incubation at 37 °C, unreacted MTT and medium were removed and 100 μL DMSO was added to solubilize the formazan crystals. The 96-well plate was read on a microtiter plate reader (Miles Inc. Titertek Multiscan Plus MK II) at an absorbance of 560 nm. The results were plotted as percent survival of the corresponding dark (drug no light) control for each compound tested after subtracting medium only control absorbance. Drug dose−cell survival curves were generated (using Microcal Origin 6.0) and LD_{50} value was measured on the curve based on Gaussian and Sigmoidal fitness. Each data point represents the mean from 3 separate experiments with 6 replicates at each dose, and the standard errors were less than 10%

Method for *in Vitro* Drug Uptake. Drug uptake was determined in RIF cells grown as described above. Approximately 1.5×10^5 cells per well were seeded in 6-well plates. After an overnight incubation at 37 °C the medium was aspirated and fresh medium (3 mL/well) was added. The photosensitizers at 0.25 μM were added (3 wells/photosensitizer) and incubated in the dark at 37 °C for 3 and 24 h. Drug-containing medium was removed; cells were washed with PBS (without Ca^{2+}), and 1 mL of Solvable (PerkinElmer Life and Analytical Sciences) was added to each well to solubilize the cells. The plates were incubated in the dark at 37 °C for 2 h. After the incubation time, 2 mL of ddH_2O was added to each well and the fluorescence was read (ex. 415 nm; em. 700 nm) on FluoroMax-2 (ISA, JOBIN YVONSPEX, Horiba Group). The protein content of the 3 mL sample was determined using the Bio-Rad DC Assay. The data was plotted as fluorescence units/mg/mL of protein.

Method for Investigating Intracellular Localization. RIF cells were grown on poly-L-lysine coated coverslips in 6-well plates, and incubated in growth medium for 3 and 24 h with compounds **3** and **13**. Fluorescent compounds (Molecular Probes) specific for different subcellular organelles were coincubated with compounds **3** and **13** prior to examination by fluorescence microscopy (for mitochondria, Mitotracker green, 1 μM for 30 min at 37 °C; for lysosomes, Lysotracker Green, for 30 min at 37 °C; and for the Golgi apparatus, Bodipy FL C5 Ceramide in the form of bovine serum albumin (BSA) complexes, 5 μM as directed by manufacturer's protocol for 30 min at 37 °C). Cells were washed twice with PBS prior to examination using a Zeiss Axiovert 200 Inverted microscope, with a Fluoarc mercury vapor shortarc lamp as light source. Images were collected with the AxioCam MR-MRGrab Frame grabber and processed with AxioVision LE 4.1 Imaging Software. The individual fluorochromes were examined with the following filter combinations from ChromaTechnology: for compounds **3** and **13**, Ex BP D410/40, BeamSplitter FT 505dcxvu, Em BP 675/50; for MTG and Lysotracker Green, Set 38 1031-346, Ex BP 470/40, BeamSplitter FT 495, Em BP 525/50; for Bodipy C5 Ceramide, Set 31 1031-350, Ex BP 565/30, BeamSplitter FT 585, Em BP 520/60.

Procedure for Evaluating *in Vivo* Photosensitizing Efficacy. The C3H/HeJ mice were intradermally injected with 2×10^5 RIF cells in 30 mL of HBSS without Ca^{2+} and Mg^{2+} on the flank, and tumors were grown until they reached 4−5 mm in diameter. The day before laser light treatment, all hair was removed from the inoculation site and the mice were injected intravenously with varying photosensitizer concentrations. At 24 h postinjection, the mice were restrained without anesthesia in plastic holders and then treated with laser light from a dye laser tuned to emit drug-activating wavelengths. The treatment parameters consisted of an irradiated area of 1 cm^2, a fluence rate of 75 mW/cm^2 for a dose of 135 J/cm^2. The mice were observed daily for signs of weight loss, necrotic scabbing, or tumor regrowth. If tumor growth appeared, the tumors were measured using two orthogonal measurements *L* and *W* (perpendicular to *L*) and the volumes were calculated using the formula $V = (L \times W^2)/2$ and recorded. Mice were considered cured if there was no sign of tumor regrowth by day 90 post PDT treatment.

Molecular Modeling

Structure of Ligands. The structures of compounds **3**, **4**, and **5** are built from the crystal structure of benzimidazolo-[2,1-*n*]purpurin-18−13^1-imino-13^2-imide methyl ester (CSD-ID FOXTUH).[34] Appropriate modifications were performed with the SYBYL modeling program version 7.1 (Tripos Inc., St. Louis, MO) using standard geometry and the SYBYL fragment library. The extended conformation was assumed for the linker region as well as substituents on the chlorine ring. The geometry of each compound was fully energy optimized with a semiempirical molecular orbital method, AM1, using the SPARTAN02 software (Wavefunction Inc., Irvine, CA).

Structure of Galectin−Ligand Complexes. (a) Construction of the Galectin−Purpurinimide−Lactose Conjugates. The high-resolution crystal structure of human galectin-3 carbohydrate recognition domain complexed with *N*-acetyllactosamine (PDB code 1A3K[35]) was used as a

template to model galectin-3 purpurinimide−lactose conjugate complexes. Similarly, the crystal structure of lactose human galectin-1 complex (PDB code 1GZW[36]) was used to guide the placement of the purpurinimide−lactose conjugates. The purpurinimide and linker moieties of the AM1 energy optimized structures of the compounds **3**, **4**, and **5** were placed into the carbohydrate binding site of galectin-1 and galectin-3. The 4 glucose atoms at the conjugation site, (C1, C2, O1, and O5) were used as the references for superposition operations. Appropriate modification was made to create a composite of the crystal lactose and AM1 optimized purpurinimide linker to form the purpurinimide−lactose conjugate molecules at carbohydrate binding site of galectins.

(b) Conformational Search of the Purpurinimide−Lactose Conjugates at Carbohydrate Binding Site of Galectins. The preliminary conformational search of purpurinimide−lactose conjugate on the galectin carbohydrate binding site was performed with the use of the "systematic search" module of Tripos SYBYL molecular modeling software. Due to its limitations, only Tripos Force field was available with the "systematic search" module. The MMFF94 charges were used for the electrostatic interaction. Three torsional angles in the linker between the lactose and purpurinimide and an additional 10 torsional angles from 3 purpurinimide substituents, i.e., the *N*-hexyl substituent, the methyl ester substituent at position 17, and the ethyl group at position 3 (for compound **4**) or at position 8 (for compounds **3** and **5**), were examined. Thus a total of 13 angles were systematically modified with the default set-up at 30 degree intervals. The torsional angles and energy of interactions between purpurinimides and the galectin residues were computed. The results were analyzed with the Tripos SYBYL analysis systematic search module, which produced a table of all conformers within the preset cutoff, each row containing all the torsional angles and the corresponding energy. From the table, the lowest energy conformer was selected from each group of conformers representing a specific conformation of the linker region and was subjected to the energy optimization. Both galectin protein atoms and galactose atoms are fixed in space and only atoms that belong to glucose, linker, and purpurinimide are allowed to move in the environment of the binding site. Since Tripos force field often produce a distorted chlorin ring without the central metal ions (results not shown), the MMFF94 force field, MMFF94 atomic charges, distance dependent dielectric function, and nonbonding cutoff of 8 Å were used for the minimization process. Standard default options were used for the minimization process. Similar energy minimization was performed with the lactose−galectin complex crystal structures as the reference with only the glucose moiety used for optimization. The interaction energy between the galectin and the ligand was calculated as the difference between the complex energy and a sum of isolated constituent (protein and ligand) energy using MMFF94 force field, MMFF94 atomic charges, distance dependent dielectric function, and nonbonding cutoff of 8 Å.

Acknowledgment. The financial support from the NIH (CA55791), Roswell Park Alliance Foundation and the shared resources of the RPCI support grant (P30CA16056) is highly appreciated.

MP060135X